
An Assessment of Short-medium Term Interventions Using CAESAR-Lisflood in a Post-earthquake Mountainous Area

Di Wang^{1,2,3}, Ming Wang¹, Kai Liu¹, Jun Xie¹

¹School of National Safety and Emergency Management, Beijing Normal University, Beijing, China.

²Academy of Disaster Reduction and Emergency Management, Beijing Normal University, Beijing, China.

³Faculty of Geographical Science, Beijing Normal University, Beijing, China.

Correspondence to: Ming Wang (wangming@bnu.edu.cn)

Abstract. The 2008 Wenchuan earthquake ~~rapidly~~ triggered rapid local geomorphic changes, shifting abundant material through exogenic processes and ~~creating/generating~~ vast amounts of loose material. The substantial material ~~dynamics/movement~~ increased the ~~risks of~~ geo-hazards (flash floods, landslides, and debris flows) risks induced by extreme precipitation in the area. Intervention measures such as check dams, levees, and ~~vegetation revetments~~ vegetated slopes have been constructed in specified sites/specific locations to reduce sediment transport, ~~thus mitigating and thereby mitigate~~ the risk/impact of ensuing geo-hazards.

This study assessed the short-medium term effects of ~~various~~ interventions, ~~incorporated with/including~~ multiple ~~facilities, on~~ control measures, in a post-earthquake fragile mountains in the short-medium-term mountainous region. Taking the Xingping valley as an example, we used CAESAR-Lisflood-~~software~~, a two-dimensional landscape evolution model, to simulate three scenarios: ~~unprotected landscapes, present protected landscapes~~ Unprotected Landscape, Present Protected Landscape, and ~~enhanced protected landscapes~~ Enhanced Protected Landscape between 2011 and 2013. We defined two ~~indicators/indices~~ to assess the intervention effects of the three scenarios by comparing the geomorphic changes and sediment yields.

The results show that the mitigation ~~facilities/measures~~ are effective, especially the geotechnical engineering efforts ~~cooperat-~~ ing in combination with ~~vegetation revetments~~ ecological engineering in the upstream area. The spatial patterns of erosion and deposition change considerably due to the intervention measures. Additionally, the effectiveness of each intervention scenario shows a gradual decline over time ~~caused directly by, mainly due to~~ the reduction in the reservoir's storage capacity. The enhanced scenario performs better than the present one, with a smaller/more gradual downward trend of effectiveness. The simulation results ~~assessevaluated~~ the ability and effectiveness of ~~cooperated~~ comprehensive control measures and will support ~~optimum/optimal~~ mitigation strategies.

1 Introduction

Strong earthquakes can trigger co-seismic landslides, ~~discontinuously crack mountains,~~ and ~~thus discontinuous rock masses in~~ mountainous areas that can increase ~~weak structural planes/erosion~~ (Huang, 2009) ~~by weathering and erosion. Consequently,~~ material shifted from coseismic landslides and attendant mass failures caused by weakened slopes modify mountain landscapes by various surface processes for days, years, and millennia (Fan et al., 2020). The 2008 Wenchuan Ms 8.0 (the surface wave magnitude, which is the logarithm of the maximum amplitude of the ground motion of the surface waves with a wave period of 20 seconds) earthquake has been influencing towns and other infrastructure in the affected area. Many studies have mapped the landslides triggered by this devastating earthquake. One study, Gorum et al. (2011), performed an extensive landslide interpretation using a large set of high-resolution optical images and mapped nearly 60,000 individual landslides, all impacting an area of 600 m² or more. Another study, Xu et al. (2014), delineated 197,481 landslides formed by polygons, centroids, and

top points compiled from visual image interpretation. To estimate the threat of loose material in subsequent sediment disasters caused by landslides, some research has attempted to measure the volume of deposited material based on field surveys and assumptions. For example, Consequently, the movement of material through co-seismic landslides and attendant mass failures modify mountain landscapes through various surface processes for days, years, and millennia (Fan et al., 2020). The 2008 Wenchuan earthquake with a surface-wave magnitude (M_s i.e., the logarithm of the maximum amplitude of the ground motion of the surface waves with a wave period of 20 seconds) of 8.0 has influenced towns and other infrastructure in the affected area. Many studies have mapped the landslides triggered by this devastating earthquake. Gorum et al. (2011) performed an extensive landslide interpretation using a large set of high-resolution optical images and mapped nearly 60,000 individual landslides, impacting an area of 600 m² or more. Xu et al. (2014) delineated 197,481 landslides represented by polygons, centroid points, and top points compiled from visual image interpretation. To estimate the impact of loose material on subsequent sediment transport caused by landslides, some research attempted to calculate the volume of deposited material based on field surveys and assumptions. For example, Huang and Fan (2013) estimated that 400 million m³ of material was deposited in heavily affected areas by assuming that the material was deposited on steep slopes with angles larger than 30° and a catchment area of more than 0.1 km². An approximate 2,793 million m³ of sediment debris was calculated by Chen et al. (2009) using different deposited deposition depth settings in different buffer zones of the Longmenshan central fault. In summary, a tremendous amount of loose material accumulated in the gullies and on hillslopes in earthquake-affected catchments, which became available for erosion and other exogenic processes for years to come. As a result, mitigation in To mitigate the abovementioned hazards and protect the Wenchuan earthquake-stricken area is still ongoing landscape including downstream settlements, structural mitigation measures have been developed in the affected area, depending on the different site-specific conditions, in addition to technical and economic feasibilities. For example, slope protection with vegetation was conducted to stabilise source material on hillslopes (Cui and Lin, 2013; Forbes and Broadhead, 2013; Stokes et al., 2014). Check dams were also used widely to intercept upriver sediment (Yang et al., 2021; Marchi et al., 2019). Lateral walls and levees, which are longitudinal structures (Marchi et al., 2019), used to protect settlements near main channels with relatively high levels of sediment discharge. Structural mitigation measures have been developed in the affected areas depending on the different site conditions and other technical and economic feasibilities. For example, ecological mitigation, such as vegetation revegetations, was conducted to stabilise the source area in hillslopes (Cui and Lin, 2013; Forbes and Broadhead, 2013; Stokes et al., 2014), and check dams were used widely to intercept upriver sediment (Yang et al., 2021; Marchi et al., 2019). And lateral walls and levees which are longitudinal structures (Marchi et al., 2019), can be built to protect infrastructure in mountain watersheds with relatively higher sediment runoff into main streams. Although comprehensive mitigation control measures were performed at have been taken in potentially dangerous sites, disasters still occurred improving mitigation performance in the Wenchuan earthquake-stricken area is still ongoing. The seasonal and periodic occurrence of massive sediment transport often particularly affect the mountainous area. This might be caused by intense precipitation and the failure of mitigation measures due to rough terrain, vague information about source material, intensive precipitation storage, and sometimes relatively low-cost mitigation measures (Yu et al., 2010; Cui et al., 2013). (Yu et al., 2010; Cui et al., 2013). Therefore, understanding and quantifying the effectiveness of intervention measures is crucial for mitigation strategies. Some Many studies focus have focused on establishing post-evaluation effectiveness index systems that are not supported by sufficient practices (Zhang and Liang, 2005; Wang et al., 2015). Some researchers compare compared the changes before and after intervention measures by recording long-term on-site measurements, which face the challenges of needing require a great deal of time, energy and financing (Zhou et al., 2012; Chen et al., 2013) (Zhou et al., 2012; Chen et al., 2013). Recent research has More recently, studies have compared disaster characteristics before and after mitigation actions, which are quickly obtained from through quick calculations using numerical simulations (Cong et al., 2019; He et al., 2022).

79 Nevertheless, these ~~disaster characteristics studies~~ ignore the ~~long-term lasting~~ effects of earthquakes on geomorphic changes
80 (longer than the duration of a single event). Therefore, the short-medium term (from the duration of a single event to decades
81 after) ~~and spatial~~ geomorphic changes obtained from simulations provide more details to interpret engineering measures in
82 notable locations, even in locations inaccessible to humans.

83 ~~CAESAR-Lisflood (C-L), which is based on the cellular automata (CA) framework (Coulthard et al., 2013), has powerful~~
84 ~~spatial modelling and computing capabilities to simulate complex dynamic systems (Batty and Xie, 1997; Coueclis, 1997;~~
85 ~~Coulthard et al., 2002). The model enables the study of many earth system interactions under different geo-environmental.~~
86 ~~Representation of deposition and erosion within C-L is used widely in rehabilitation planning and soil erosion predictions in~~
87 ~~post-mining landforms (Saynor et al., 2019; Hancock et al., 2017; J.B.C. Lowry et al., 2019; Thomson and Chandler, 2019;~~
88 ~~Slingerland et al., 2019) as well as channel evolution and sedimentary budget planning for dam settings (Poepl et al., 2019;~~
89 ~~Gioia and Schiattarella, 2020; Ramirez et al., 2020, 2022). In addition, there have been a series of studies in mountainous area~~
90 ~~involving secondary geo-hazard driving factors (Li et al., 2018; Wang et al., 2014b) and vegetation recovery (Zhang et al.,~~
91 ~~2018). One study, Li et al. (2020) and Xie et al. (2018) used C-L with different rainfall and future climate change scenarios to~~
92 ~~interpret the landscape evolution after the Wenchuan earthquake. The methods and parameter values used in the above research~~
93 ~~helped promote this model's application in other study areas.~~

94 ~~In this study, hourly CAESAR-Lisflood (C-L), a two-dimensional hydrodynamic surface landscape evolution model based on~~
95 ~~the cellular automata (CA) framework, has powerful spatial modelling and computing capabilities (Coulthard et al., 2002; Van~~
96 ~~De Wiel et al., 2007; Bates et al., 2010; Coulthard et al., 2013a). C-L is used widely in rehabilitation planning and soil erosion~~
97 ~~predictions in post-mining landscapes (Saynor et al., 2019; Hancock et al., 2017; J.B.C. Lowry et al., 2019; Thomson and~~
98 ~~Chandler, 2019; Slingerland et al., 2019) as well as studies in channel evolution and sedimentary budget planning for dam~~
99 ~~settings (Poepl et al., 2019; Gioia and Schiattarella, 2020; Ramirez et al., 2020, 2022). The applications presented demonstrate~~
100 ~~the efficiency of C-L model to simulate the surface material migration and landscape evolution after anthropogenic and natural~~
101 ~~disturbances, which indicate the potential to simulate the complexity of surface processes integrated with different interven-~~
102 ~~tions. In addition, many studies applied C-L to investigate the landscape evolution after the Wenchuan earthquake (Li et al.,~~
103 ~~2020; Xie et al., 2022a, b, 2018). The configuration of the model can be referenced to the study of intervention scenarios in~~
104 ~~the same post-earthquake region.~~

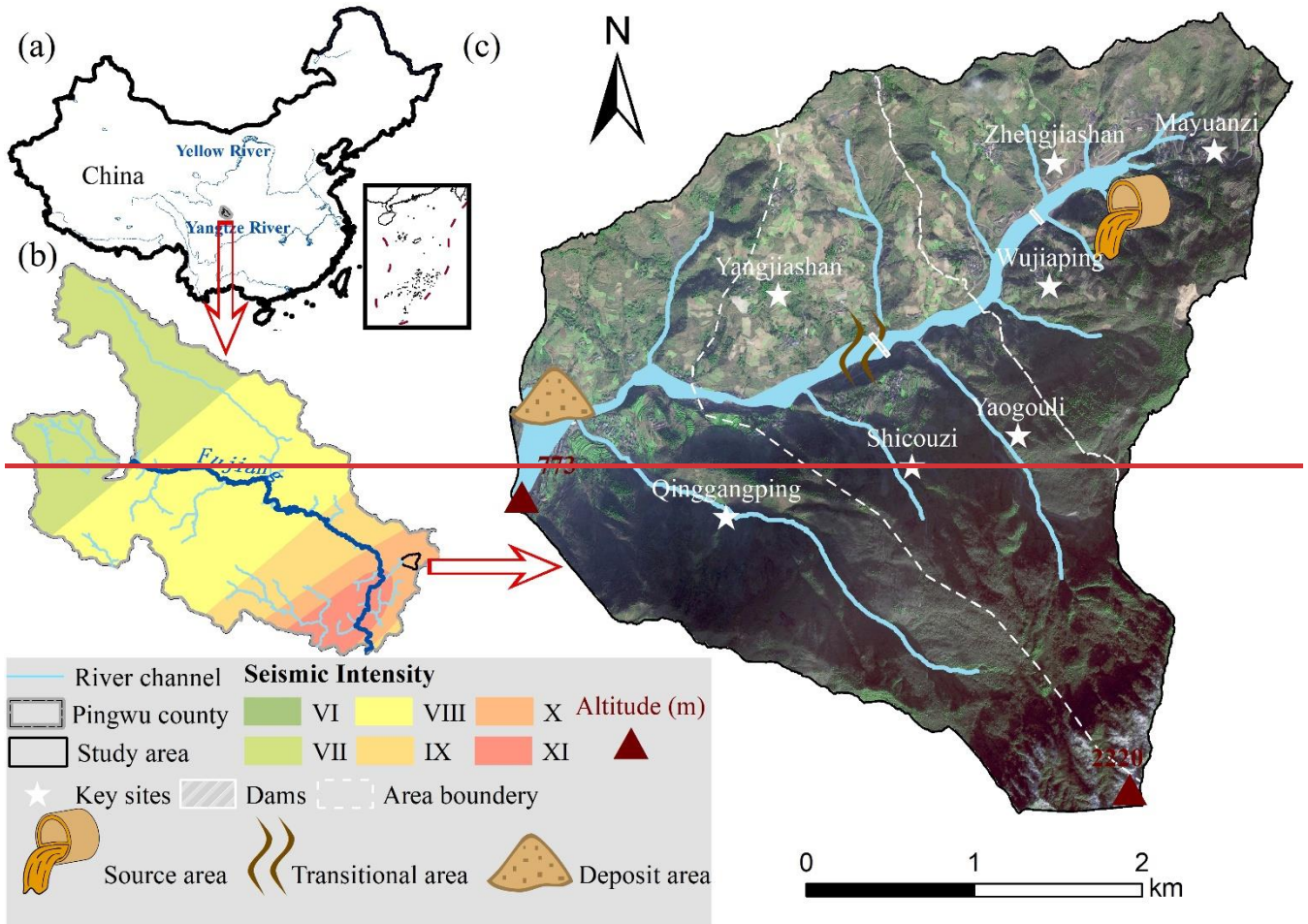
105 ~~In this study, we investigated the impact of different interventions on sediment dynamics and geomorphic changes in an earth-~~
106 ~~quake-stricken valley. Hourly rainfall data over three years were generated by daily downscaling to capture extreme events.~~
107 ~~Based on the input data, we We then~~ simulated and compared the geomorphic changes and sediment yield in three scenarios
108 that varied in their mitigation compositions and intensities in the catchment. The objectives were 1) to assess the effectiveness
109 of a set of mitigation ~~facilities measures~~ to reduce sediment transport, 2) to analyse the role of each ~~facility measure~~ on geo-
110 morphic changes, and 3) to determine the influence of vegetation on catchment erosion.

111 2 Study area

112 2.1 Regional characteristics

113 The study area was the Xingping valley ~~in north-eastern Sichuan Province~~, the left branch of the Shikan River (a tributary of
114 the Fu River) ~~in north-eastern Sichuan Province~~ (Fig. 1). ~~There are nearly~~ Nearly two hundred ~~households settlements~~ scattered
115 ~~among more than five villages~~ in the ~~study~~ catchment. The ~~topography of the catchment is rugged, with an elevation between~~
116 ~~800 and 3036 m and anhas a total drainage~~ area of approximately 14 km². ~~The catchment- and a rugged topography with an~~
117 ~~elevation ranging from 800 to 3036 m, which~~ is characterised by a high longitudinal gradient (~ 120%) and ~~distributed~~ more

118 than ten small V-shaped branch gullies. ~~The length from the northeast to the southwest is 5,770 m, and the width is 4,150 m in~~
 119 ~~the perpendicular direction.~~ The region has a humid temperate climate with a mean annual temperature of 14.7 °C. The mean
 120 annual precipitation is 807.6 mm, ~~mainly with more than 80% concentrated~~ between May and September. The steep terrain and
 121 ~~short-term~~ heavy rainfall ~~dominate~~ are combined to control the nature of the ephemeral streams in this area.
 122 The local basement rocks are mainly metamorphic sandstones, sandy slate, crystalline limestone, and phyllite of the Triassic
 123 Xikang Group (T_{3xk}) and Silurian Maoxian Group (S_{mx}), which are easily worn away by quick weathering in static processes
 124 after disturbs caused from strong earthquakes. Consequently, the Wenchuan earthquake, with a Modified Mercalli Intensity
 125 scale of X, made this area one of the most severely affected locations (Wang et al., 2014a) and produced 10^6 m^3 loose material
 126 by triggering landslides and subsequent weathering in Mayuanzi, Zhengjiashan, and Wujiaping (Fig. 1) The basement rocks in
 127 the study area are mainly metamorphic sandstone, sandy slate, crystalline limestone, and phyllite of the Triassic Xikang Group
 128 (T_{3xk}) and Silurian Maoxian Group (S_{mx}), which are easily eroded by in situ weathering processes after disturbances caused by
 129 strong earthquakes. Consequently, the Wenchuan earthquake, with a Modified Mercalli Intensity scale of X, made this area
 130 one of the most severely affected regions (Wang et al., 2014) and produced 10^6 m^3 of loose material by triggering landslides
 131 and subsequent erosion in Mayuanzi, Zhengjiashan, and Wujiaping (Fig. 1) (Guo et al., 2018).



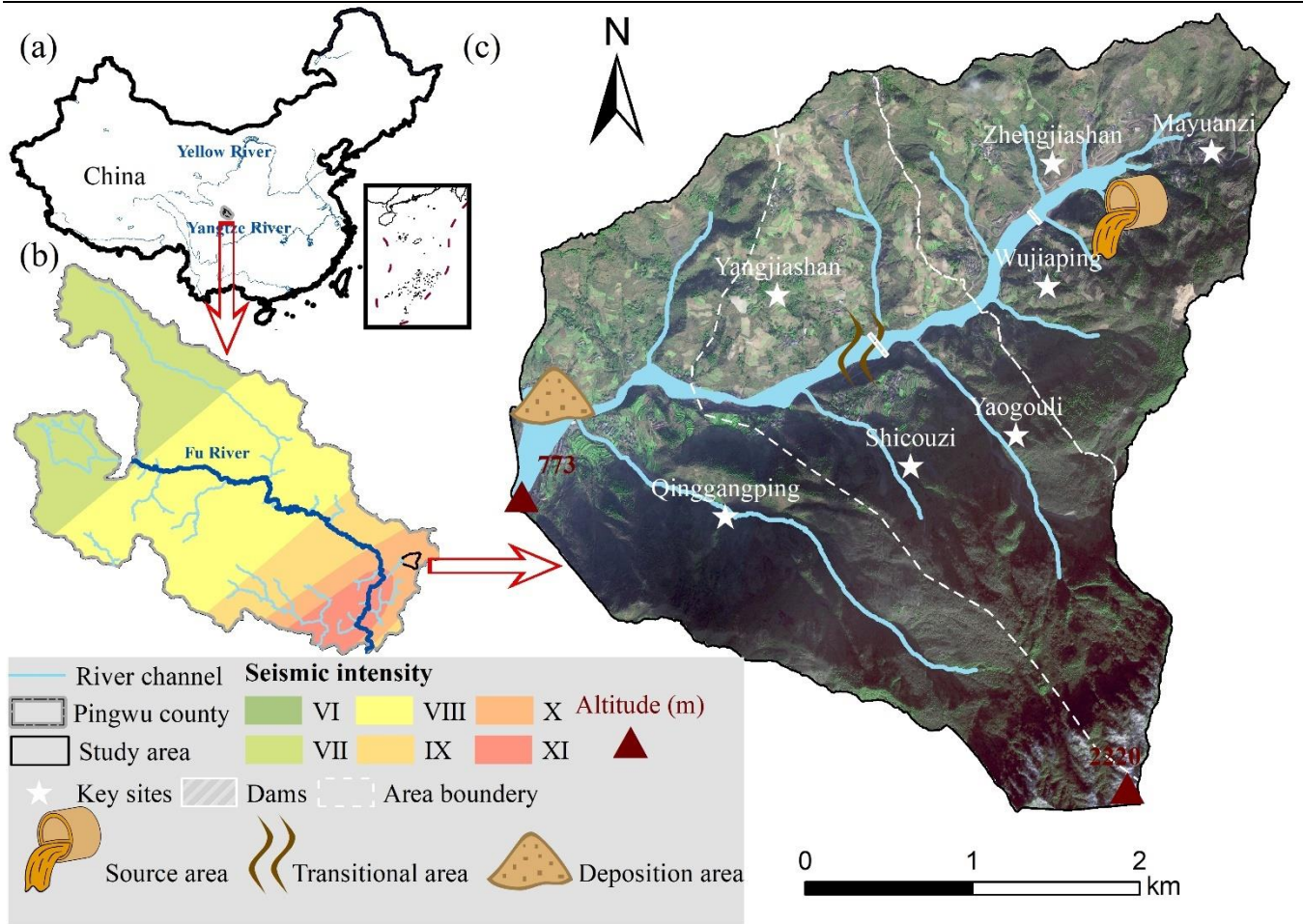


Figure 1: An overview of the study area. (a) The location of the study area; (b) A seismic intensity map of the Wenchuan earthquake within Pingwu County; (c) A schematic image of the study area.

2.2 Historical hazards and intervention measures

Six debris flow-flash flood disaster chain groups have been found in the Xingping valley over the decade after the earthquake. Based on the published work of SKLGP (State Key Laboratory of Geohazard Prevention and Geoenvironment Protection) and the local states' geological survey before 2018 of local government and our biannual field surveys since 2012, we catalogued the time of occurrence, total rainfall of each event, and corresponding disaster details of each event (Table S1). The massive amount of sediment was transported quickly soon after the devastating earthquake in 2008 and 2009, and extensive loose materials were then delivered and deposited in the channel triggered by the extreme rainfall events in 2013 and 2018 triggered the deposition of extensive loose material in the channel. Considering the transport processes of landslide process material, we divided the study area into three regions subregions: the source area, the transitional area, and the deposit deposition area (Fig. 1). The white dashed lines in Fig. 1c, indicate that the loose solid material can be easily be transported from the source area to the deposit deposition area through the transitional zone.

An engineering control project was constructed in the study valley to intercept the upriver material in October 2010. The project included two check dams, with one located in the upper source area and the other located in the transitional zone (Feng et al., 2017) (Feng et al., 2017) (Fig. 1c). The upper dam has a storage capacity of $5.78 \times 10^4 \text{ m}^3$ and a height of 10.0 m. The dam at transitional area dam has a storage capacity of $7.2 \times 10^4 \text{ m}^3$ and a height of 9.0 m. With the reservoirs gradually filling with deposits, the first dredging work was subsequently performed in 2013 due to gradually filling of the reservoirs. Nearly three years later, the storage capacity behind the upper dam remained at 50% in 2016, while the transitional area dam could no longer retain sediment.

3 Materials and Methods

In this study, we examined the intervention effectiveness through the morphological response and sediment yield in the Xingping valley, which was simulated using the C-L models simulations. The research entailed four main steps: 1) setting three scenarios with different intervention compositions measures, 2) preprocessing the model input data, including three groups of DEMs, the rainfall data, and the m value of the C-L, 3) calibration of the hydrological component, and 4) simulating landscape geomorphic changes and analysing the intervention effectiveness during 2011-2013.

3.1 Scenario settings

The abundant source-material triggered mobilised by landslides should be controlled to prevent reduce the threat of disasters downstream sediment transport. Therefore, we designed three scenarios by incorporating integrating geotechnical engineering and biological measures referenced to current facilities with ecological engineering to assess the effectiveness of intervention measures. Scenario UP: Unprotected landscapes meant unprotected landscape means the sediment would be transported without anthropogenic intervention. Scenario PP: Present present protected landscapes implied landscape means that only the present two check dams trapped sediment during 2011-2013 without dredging work over this period (see Section 2.2). Scenario EP: Enhanced enhanced protected landscapes emphasised landscape represents the addition of slope protection with vegetation revetments in the source area and levees in the deposit deposition area based on, in addition to the two check dams in Scenario PP.

Figure 1c shows the locations of the existing two check dams in both Scenario PP and Scenario EP. We determined the placements of additional facilities in Scenario EP according to the field survey, which demonstrated that the continuous supply of sediment was mainly from the source area. Therefore, vegetation revetments such as tree planting would be carried out upstream to prevent erosion by stabilising the topsoil and enhancing the soil's infiltration capacity via roots (Lan et al., 2020). Considering the damage caused by flash floods to the residential area downstream, the levees (see Fig. Figure 1c shows the locations of the existing two check dams in both Scenario PP and Scenario EP. We determined the placements of additional measures in Scenario EP according to a field survey, which demonstrated that the continuous supply of sediment is mainly from the source area. Therefore, vegetated slopes were designed in the upstream area to prevent erosion, by stabilising the topsoil and enhancing the soil's infiltration capacity via roots (Lan et al., 2020). Considering the damage caused by flash floods to the residential area downstream, the levees (see Fig. S1 and Section 3.2.2) are), i.e., artificial barriers, were placed to protect agricultural land and buildings, which help to prevent by preventing water and sediment from overflowing and flooding surrounding areas. Table 1 shows the scenario descriptions, initial model conditions and input rainfall series. The details about the model and input data are introduced below in Section 3.2.

Table 1: Scenario settings

Scenario	Descriptions	Period	DEM (10 m)	Rainfall data
UP	no anthropogenic intervention		UP DEM UP bedDEM	downscaled hourly precipitation over the period
PP	the present two check dams upstream without dredging work additional vegetation revetments vegetated slopes in the source area and levees in the deposit deposition area based on Scenario PP	2011-2013 (3 years)	PP DEM PP bedDEM	(lumped) downscaled hourly precipitation over the period (spilt)
EP			EP DEM EP bedDEM	

3.2 CAESAR-Lisflood

The C-L integrated the Lisflood-FP 2D hydrodynamic flow model (Bates et al., 2010) with the CAESAR landscape evolution model (LEM) (Coulthard et al., 2002; Van De Wiel et al., 2007)(Coulthard et al., 2002b; Van De Wiel et al., 2007), which is described in detail by Coulthard et al. (2013), Coulthard et al. (2013). The catchment mode of C-L was applied in this study, in which the surface digital elevation model (DEM), the bedrock DEM, (bedDEM), the grain size distribution, and a rainfall time series are required to simulate the geomorphic changes and sediment transport and geomorphic changes. There are four primary modules within C-L operated that are implemented as follows:

(1) a hydrological module generates surface runoff from rainfall input using an adaptation of TOPMODEL (topography-based hydrological model) (Beven and Kirkby, 1979),

(2) a hydrodynamic flow routing module based on the Lisflood-FP method (Bates et al., 2010) which calculates the flow depths and velocities,

(3) an erosion and deposition module uses hydrodynamic results to drive fluvial erosion by either the Einstein (1950) or the Wilcock et al. (2003) equations, which are applied to each sediment fraction over nine different grain sizes,

(4) and a slope model of the movement module of material movement from the hillslope into the fluvial system by considering, taking into account both the mass movement when a critical slope threshold is exceeded and soil creep processes whereby, where sediment flux is linearly proportional to the surface slope.

The C-L model updates variable values stored in square grid cells at intervals, such as DEM, grain size and proportion data, water depth, and velocity. For the three scenarios, the initial conditions, such as DEMs and bedrock DEMs, the DEM, bedDEM, rainfall data, and the m values, were preprocessed/pre-processed as follows.

3.2.1 The surface and bedrock digital elevation models

To clearly describe the control process, especially the two dams and levees in the catchment, we unified grid cell scales to 10 m for all input data of the C-L. The GlobalDEM product with a 10 m × 10 m resolution and 5 m (absolute) vertical accuracy were used to form three types of initial DEMs (UP DEM, PP DEM, and EP DEM). Before rebuilding the initial DEMs, we filled the sinks of the original GlobalDEM based on the Environmental Systems Research Institute's (ESRI's) ArcMap (ArcGIS, 10.8) to eliminate the 'walls' and the 'depressions' in the cells and thus avoided intense erosion or deposition in the early run time. Then, the non-sink/modified DEM was used as the surface DEM in Scenario UP (UP DEM) without any facilities/mitigation measures. According to the engineering control project described in Section 3.2.2, the surface DEM of Scenario PP (PP DEM) included the dams by raising the grid cell elevations by 10 m for the dam in the upper stream source area and 9 m for the dam in the transitional area/zone. Similarly, the surface DEM in Scenario EP (EP DEM) included the dams in the PP DEM. In addition, two levees were produced by raising the grid cell elevation by 2 m, representing at selected locations. For scenario EP, the placement and setting of the vegetation revetments/protection are introduced in Section 3.2.2.

The spatial heterogeneity of the source material (Fig. 1c) indicates the discrepancy/results in differences in the erodible thickness, which equals the difference between the surface DEM (DEM) and the bedrock DEM (bedDEM). We divided the study area into five regions according to the erodible thickness (Fig. S1) by checking the relative elevation of the foundations of buildings, the exposed bedrock, and the deposition depth of landslides with respect to ground level. The average thicknesses of upstream low- and high-altitude/elevation areas were set to 10 m and 3 m, respectively, and the thickness of the erodible layer in the downstream area was set to 3 m. For the river channel and outlet, as where there would be a large amount of deposition, the thickness of erodible sediment was set to 5 m and 4 m, respectively. As the dams in Scenario PP and the levees in Scenario EP were non-erosive/erodible concrete, we set the erodible thickness of these features to 0 m. Eventually, the DEM data were formatted to ASCII raster data as required by C-L. The divided regions varied in erodible thickness, the placement

of additional levees and ~~vegetable revetments~~ vegetated slopes in Scenario EP, ~~and the pre-processes of the generation process~~
of DEMs and bedDEMs are shown in Fig. S1.

3.2.2 Vegetation settings

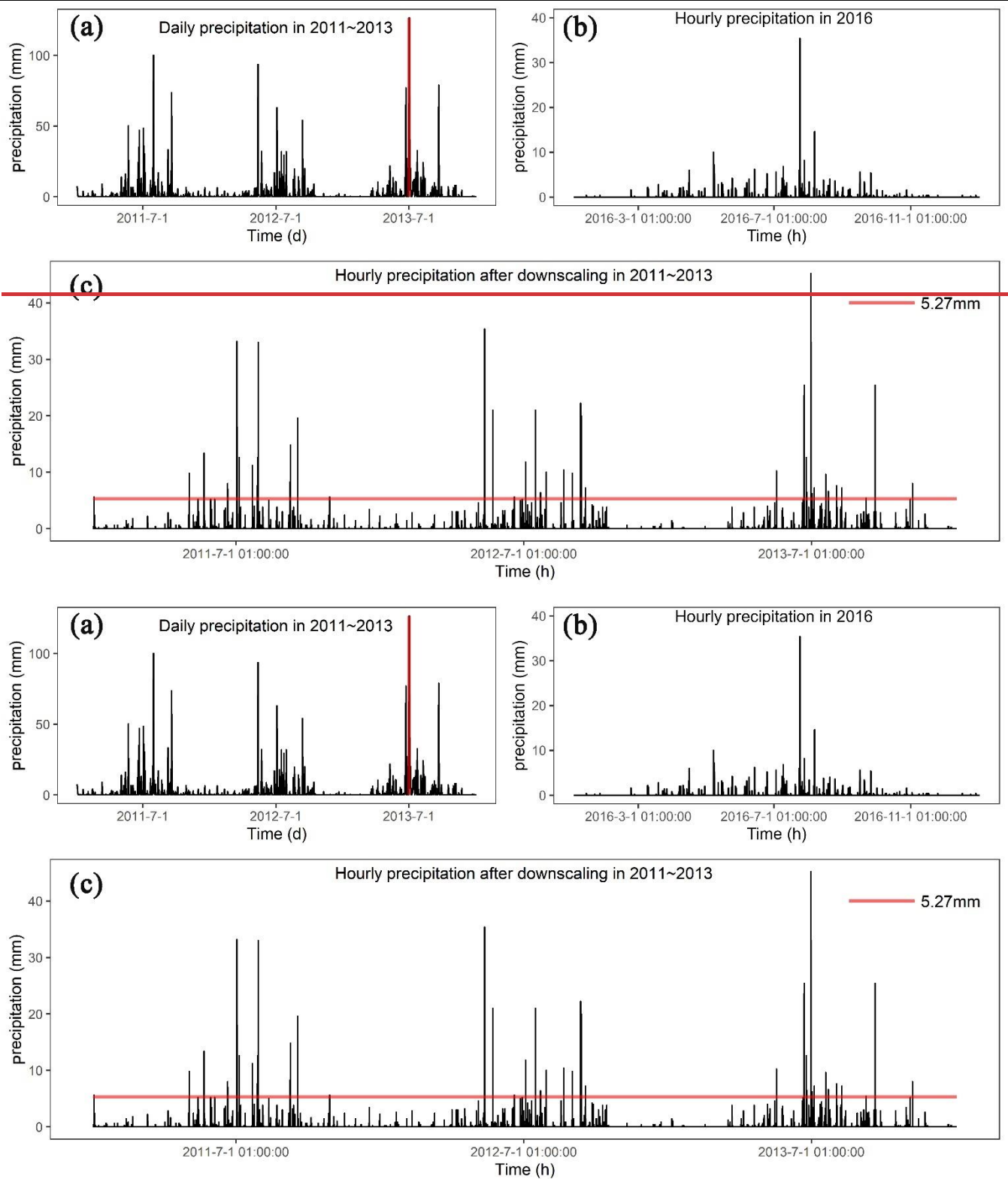
Another parameter required in each scenario simulation was the m value of the hydrological model (TOPMODEL) within C-
L, which controls an exponential decline in transmissivity with depth (Beven, 1995, 1997) and influences
the peak and duration of the hydrograph in response to rainfall. The m value effectively imitates the effect of vegetation ~~on,~~
which controls the ~~movement and storage~~ fluctuation of ~~water within~~ the soil. ~~The lower moisture deficit and thus influences~~
~~the m value is, the lower the vegetation coverage, and the higher the flash flood peak and the shorter the duration~~ of the
modelled flood hydrograph ~~is reflected~~ (Coulthard et al., 2002) (Coulthard et al., 2002b). The m value is usually determined
by the land cover (e.g., 0.02 for forests and 0.005 for grasslands) (Coulthard and Wiel, Van De J., 2017) (Coulthard and Wiel,
Van De J., 2017). In our study, we set the m value ~~asto~~ 0.008 in ~~our smaller~~ the catchment (14 km²) in Scenarios UP and PP,
which resembles the m value of farmland ~~covered~~ with lower vegetation ~~coverage in the same catchment~~ cover studied by Xie
et al. (2018) and Li et al. (2018) (Xie et al. (2018) and Li et al. (2018)). As mentioned earlier, the upstream ~~low~~ low-elevation area
~~covered~~ protected by ~~the biological measures~~ vegetation in the EP scenario was assigned a higher m value of 0.02. This m value
was calibrated by the more extensive catchment containing our study area in the flood event of 2013 (Xie et al., 2018).

3.2.3 The rainfall data

In this research, we compared three scenarios by matching precipitation data between 2011 and 2013, as mentioned in Section
3.1. The source data of precipitation in 2011-2013 (Fig. 2a) were obtained from the China Meteorological Administration
(<http://data.cma.cn>) with daily temporal resolution. The intensity and frequency of extreme rainfall events affect patterns of
erosion and deposition (Coulthard et al., 2012b; Coulthard and Skinner, 2016) (Coulthard et al., 2012b; Coulthard and Skinner,
2016). Therefore, we used the stochastic downscaling method to generate hourly data to better capture the hydrological events
introduced by Li et al. (2020) (Li et al. (2020)) and Lee and Jeong (2014) (Lee and Jeong (2014)). The referenced hourly precipi-
tation was observed from the pluviometer located 20 km from the study area in 2016 (Fig. 2b), with an annual total precipitation
of 684 mm. The observed rainfall in 2016 was characterised by (1) hourly precipitation between 1.1 mm and 35.4 mm and (2)
~~the~~ maximum and average durations of rainfall events ~~as of~~ 24 h and 2.8 h, respectively. The main processes of the downscaling
method are as follows:

- extracting the hourly rainfall of specific days in 2016 closest to the daily rainfall in 2011-2013 through the threshold setting and producing the genetic operators using the extracted hourly rainfall dataset;
- mixing the genetic operators by an algorithm (Goldberg, 1989) composed of reproduction, crossover and mutation and repeating these processes until the distance between the sum of hourly rainfall and the actual daily rainfall was less than the set threshold;
- normalising the hourly precipitation to keep the daily rainfall value unchanged.

Figure 2c shows the downscaled rainfall series between 2011 and 2013. The downscaled hourly rainfall better captured the hydrological events at an hourly scale compared to the hourly mean rain (5.27 mm) on the day with extreme rainfall (126.5 mm), which was far from the actual situation. Corresponding to the m value settings, the input of generated hourly precipitation was lumped catchment ~~lumped wide~~ in Scenario UP and Scenario PP and divided into two separate but identical rainfall events in Scenario EP.



262

263

264 **Figure 2: (a) Daily precipitation in 2011-2013 (the red vertical line indicates the maximum daily precipitation of 126.5 mm); (b)**
 265 **Hourly precipitation in 2016; (c) Downscaled hourly precipitation in 2011-2013 (the red horizontal line indicates the hourly mean**
 266 **precipitation of 5.27 mm on the day with the maximum precipitation marked in (a)).**

267 **3.2.4 Other parameters**

268 The C-L model is sensitive to a set of input dataAs introduced by Skinner et al. (2018), the C-L model is sensitive to a set of
 269 input data for a catchment with a grid cell size of 10 m, such as the sediment transport formula, slope failure threshold, and
 270 grain size set. The grain size distribution of sediment was derived from sampleingsampling at 14 representative locations in

the same study basin by ~~Xie et al. (2018)~~Xie et al. (2018). Given the grain size distribution in this study, the Wilcock and Crowe formula was selected as the sediment transport rule, which was developed from flume experiments using five different sand-gravel mixtures with grain sizes ranging between 0.5 and 64 mm (Wilcock et al., 2003). Considering the steep slopes on either side of deep gullies, a higher slope failure threshold was determined to replicate the geomorphic changes between 2011 and 2013. Additionally, we found that the probability of shallow landslides increased with increasing slope gradient from 20° to 50° ~~in slope gradients~~ between 2011 and 2013 (~~Li et al., 2018~~)(Li et al., 2018). The slope angle was derived from the DEM with a 30 m spatial resolution, which caused a lower slope angle than that with a 10 m resolution. As such, we set the slope angle ~~asto~~ 60°, which is lower than the 65° used in a scenario without landslides (Xie et al., 2022) and higher than 50°. Some parameters were determined by repeated experiments, such as the minimum Q value, and the other input values were ~~referred-~~set to default values recommended by the developers (such as the maximum erosion limit in the erosion/deposition module and the vegetation critical shear stress) in <https://sourceforge.net/p/caesar-lisflood/wiki/Home/>. Table S2 in the supplemental material presents the model parameters of C-L used in this study.

3.2.5 Model calibration

~~ConsideringBecause~~ the basin was ungauged ~~basins~~ before 2015, we replicated the flash flood event in July 2018 using C-L simulations to calibrate the hydrological components. Based on Scenario PP (with two ~~eheckingcheck~~ dams), we used the two-week hourly precipitation of July 2018 as the input (Fig. S2a), which was recorded by a rain gauge located 2.5 km ~~away~~ from the catchment (Fig. S2b). The simulation results (Fig. S2c and Fig. S2d) ~~showedyielded~~ an erosion map and a maximum water depth map in Scenario PP on July 15, 2018. We selected three locations to compare the deposition and inundation in the simulation results with satellite images and photos (Fig. S3). ~~Additionally, the~~The simulated sediment thickness and water depth were close to those measured from ~~picturesthe images~~, which indicated that the flash flood event was well replicated by the C-L using the input data.

3.3 Output analysis

The C-L model outputs of each scenario include hourly water and sediment discharge at the basin outlet and EleDiffs (the difference between ~~DEMsmodelled DEM~~ at a specified time and initial ~~DEMs (EleDiffsDEM)~~). We validated the model outputs by comparing the hourly discharge and EleDiffs reflecting the depth of sediment deposition or erosion (> 0.1 m: deposition, < -0.1 m: erosion) with field survey materials. The overall temporal and spatial geomorphic changes reflected by EleDiffs under three different scenarios were used to assess the geomorphic response to interventions. To explore the geomorphic response to various control measures, we focused on the notable sites where the ~~eheckingcheck~~ dams, levees, and ~~vegetation revetments would bevegetated slopes were~~ located and recorded the depth of accumulating sediment behind the two dams. To further explore the spatial heterogeneity, we compared the volumes of deposition and erosion among the three divided regions, including the source area, the transitional area, and the ~~depositdeposition~~ area.

Based on the visual analysis and quantitative results, we defined two formulae to assess the effectiveness of the intervention. The conservation ability (Ca , Eq. (3)) was calculated based on variables in the sediment balance system (Fig. 3). The sediment volume of deposited sediment (D_n) and input sediment from the upper connected region (I_n) is equal to that of the eroded material (E_n) and the output sediment to the next part (O_n) over the same period (Eq. (1), Eq. (2)) in the system. A higher value of Ca in a specific region and scenario indicates a more effective control system.

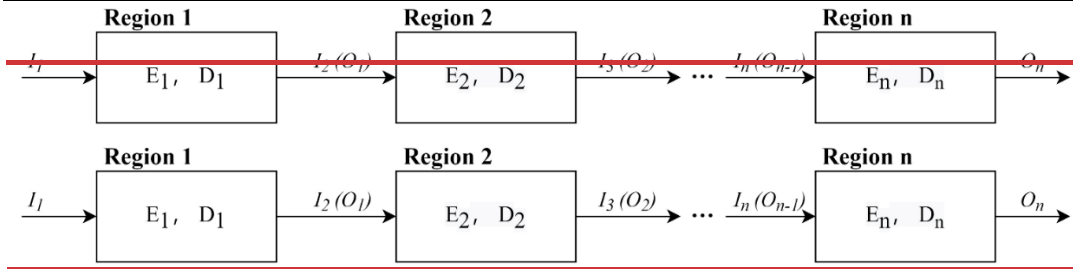


Figure 3: The sediment balance system in the study area (the Region region n indicates the source area, transitional area, and depositor or deposition area)

$$I_n = \sum_2^n E_{n-1} - \sum_2^n D_{n-1}, \quad (1)$$

$$I_n + E_n = O_n + D_n, \quad (2)$$

$$Ca = \frac{D_n}{I_n + E_n} \quad (3)$$

where n is the region number of the source area (=1), transitional area (=2), and depositor or deposition area (=3).

Additionally, we designed the relative efficiency (Re , Eq. (4)) to depict the efficiency of intervention measures in Scenario PP and EP in sediment loss, with the comparison to Scenario UP.

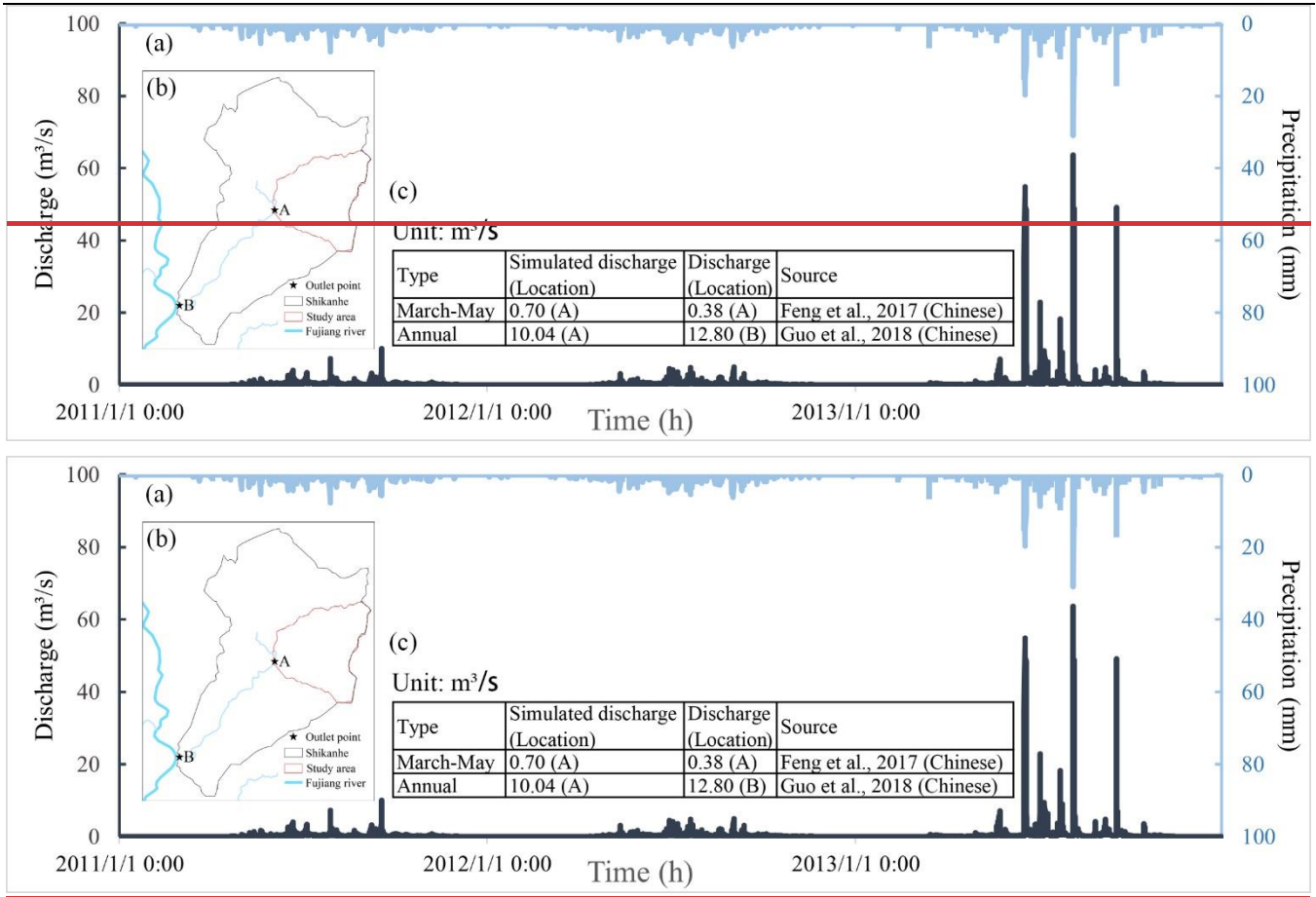
$$Re_{PP/EP,i} = \frac{Q_{UP,i} - Q_{PP/EP,i}}{Q_{UP,i}} \quad (4)$$

where i is the sequence of the day; Q_{UP} is the daily sediment yield measured at the catchment outlet in Scenario UP, and $Q_{PP/EP}$ is the same data in Scenario PP or Scenario EP of day i ; and $Re_{PP/EP}$ is the daily relative effectiveness of control measures in Scenario PP or Scenario EP.

4. Results

4.1 Model verification

Figure 4 shows the input rainfall data and modelled discharge hydrograph between 2011 and 2013 (Fig. 4a). The comparison of simulated mean discharge in April through July and the whole year with field survey materials in the two locations are also presented (Fig. 4b, c). Concerning the discharge hydrograph, the peak discharges (63.7, 54.9, and 50.3 m³/s) correspond well with the peak rainfall intensities (31, 19.7 and 15 mm). The modelled water discharge from March to May in location A is slightly larger than the measured value reported by Feng et al. (2017). Additionally, an average annual discharge of 10.04 m³/s in location A is lower than that of 12.80 m³/s in the catchment outlet (location B), which has an area approximately three times the size of the study area.



327

328

329

330

331

Figure 4: The input and output of the hydrograph. (a) The input hourly precipitation and simulated discharge in 2011-2013 in Scenario PP; (b) The locations of the specified outlet points; (c) A comparison of the simulated average discharge to the recorded discharge.

332

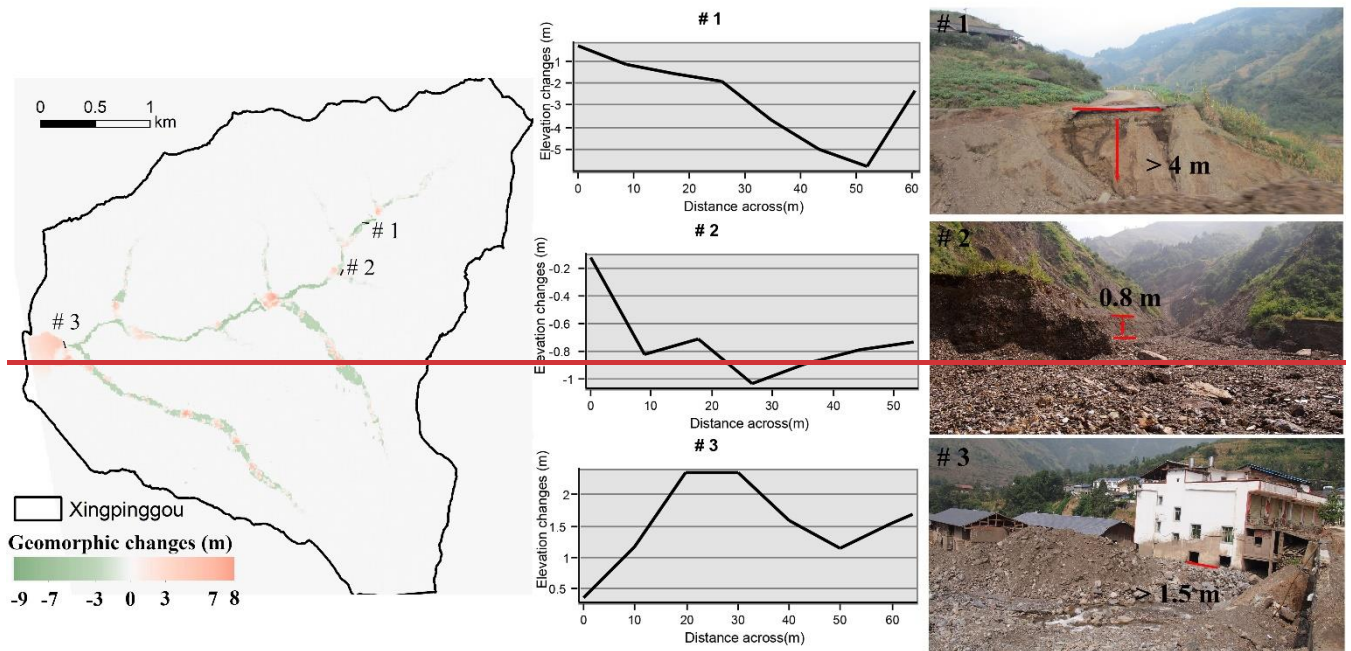
333

334

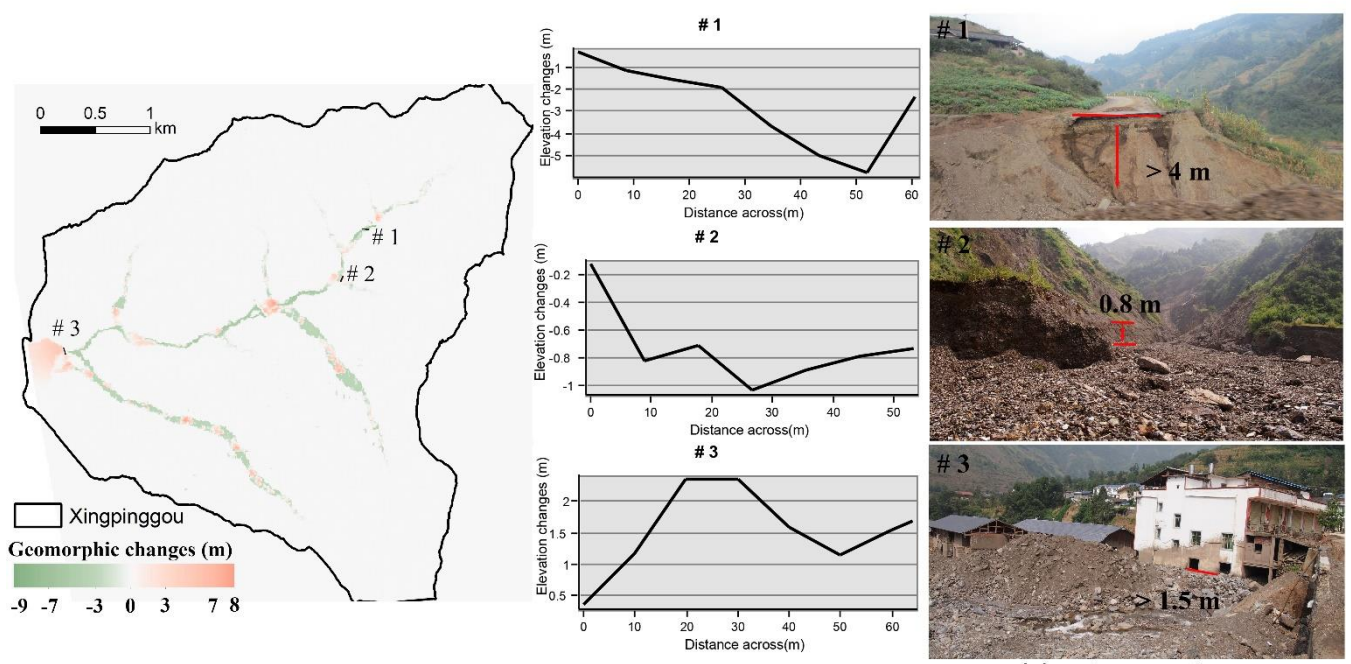
335

336

Typical cross-sections are generated (Fig. 5) based on the replicated landscape and landform changes in Scenario PP. The first site is located on the upriver road, which is eroded ~~at~~to a depth of 5.7 m according to the simulation results, while the photo shows a depth of no less than 4.0 m without an apparent eroded base. ~~The cross~~Cross-section #2 and the site photo of the gully ~~depict~~show that the eroded depth is approximately 1.0 m. Meanwhile, a clear sediment boundary is found in the building located ~~at~~in the ~~deposited~~deposition area (# 3), indicating a slightly lower deposition depth than the model predicted.



(a) the field measurement location (b) simulated elevation changes after 2013 in Scenario PP (c) photos after September 2013



(a) the field measurement location (b) simulated elevation changes after 2013 in Scenario PP (c) photos after September 2013

Figure 5: The comparison of cross-sections from the simulation results to the field measurements after 2013 in Scenario PP.

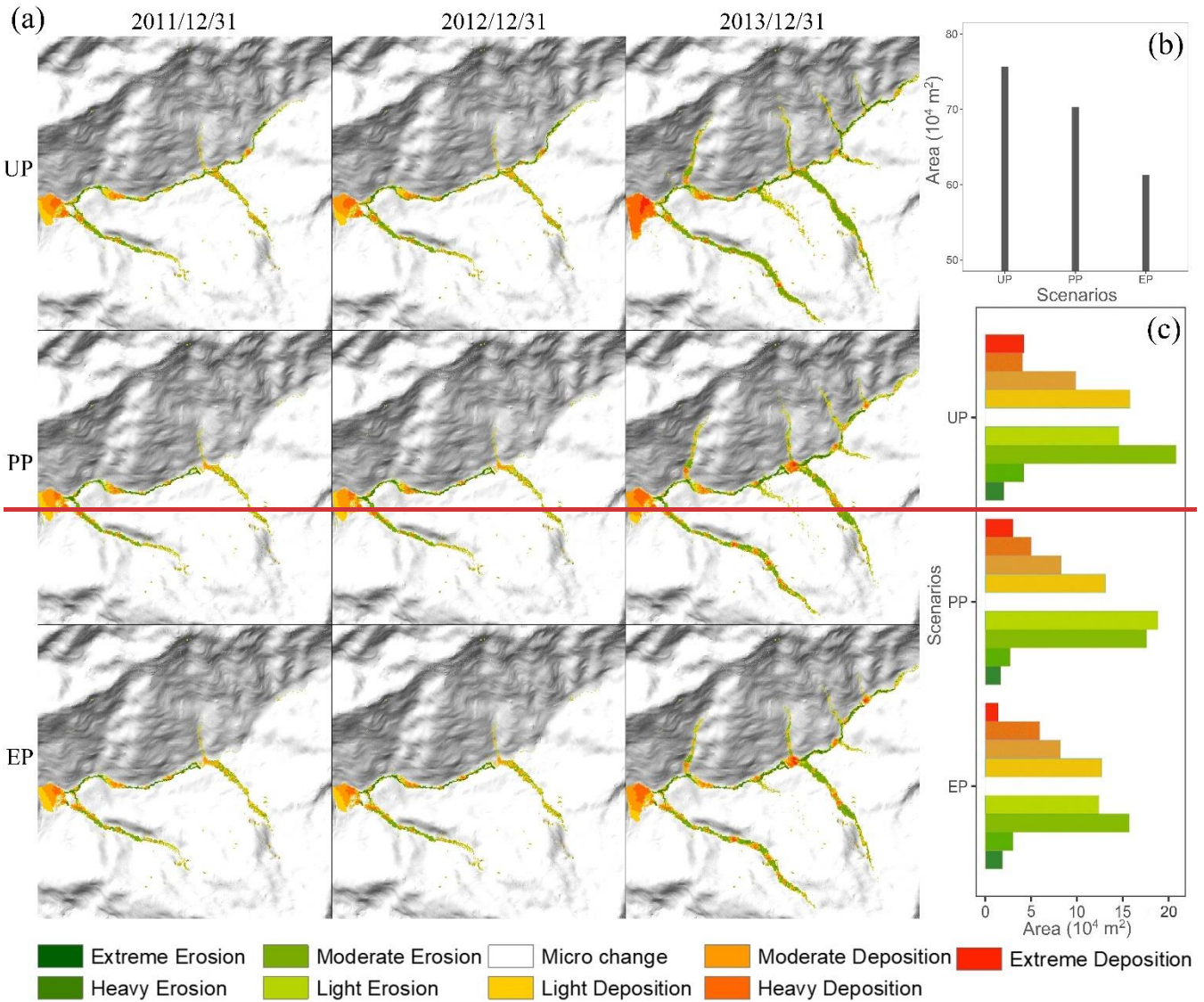
4.2 Overall geomorphic changes

Figure 6a compares the three annual **landscape/landform** changes in each scenario, which are classified into nine categories **by according to** natural breaks for EleDiffs: extreme erosion (<-7 m), heavy erosion (-7--3 m), moderate erosion (-3--1 m), light erosion (1-0.1 m), **micro/minor** change (-0.1-0.1 m), light deposition (0.1-1 m), moderate deposition (1-3 m), heavy deposition (3-7 m), and extreme deposition (>7 m). A similar spatial pattern of erosion is observed in all three scenarios. More specifically, erosion mainly emerges in the main channel and the branch valleys, among which the left branches **are exhibit** more pronounced

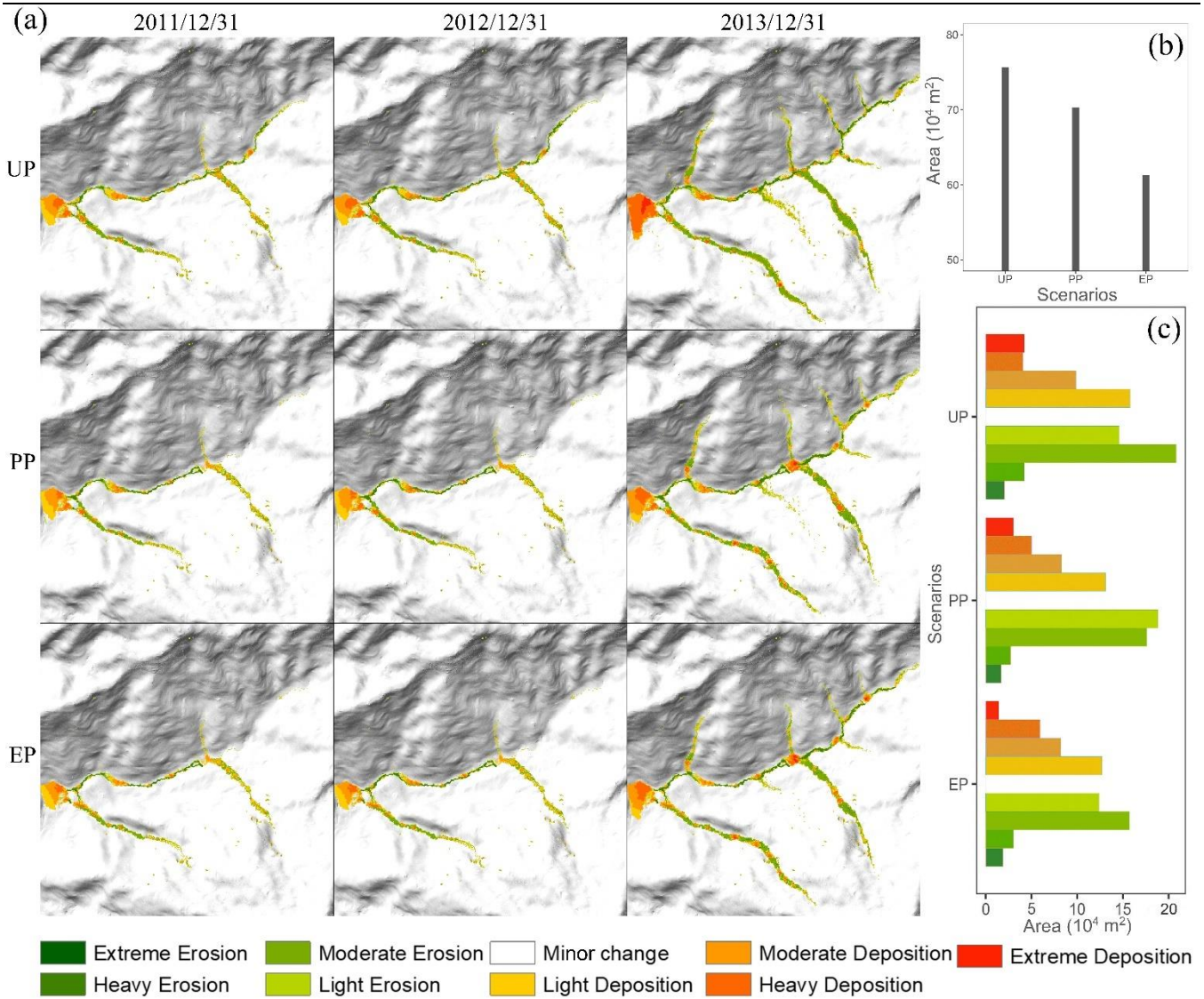
346 erosion. In contrast, the ~~depositional~~deposition zone appears to vary in the three scenarios, especially in the area behind the
 347 two dams ~~shown~~present in Scenarios PP and EP.

348 The total area of ~~affected grid cells representing~~ erosion and deposition ~~for in the~~ three scenarios ~~are is~~ calculated to compare
 349 the ~~damages~~ (Figure ~~impact of sediment transport~~ (Fig. 6b). The affected area in Scenario UP is approximately 0.76 km² (5.4%
 350 of the total catchment), which is larger than that in Scenario PP (0.70 km², 5.0% of the whole catchment), and the affected area
 351 decreases to 0.61 km² (4.4% of the total catchment) in Scenario EP. The total area of erosion and deposition decreases gradually
 352 with more controlling measures established in this study.

353 Figure 6c compares the extent of geomorphic changes in three situations using the ranges that varied in depth. The ~~erosion~~
 354 ~~area~~areas of ~~the~~light ~~one~~ and moderate ~~one is~~erosion ~~are~~ are greater than the ~~areas of~~ extreme and heavy erosion ~~area for in~~ all
 355 three scenarios. The zone of each erosion degree in UP is more extensive than that in PP, followed by that in EP. In addition,
 356 the greater the deposition depth is, the smaller the ~~area of~~ deposition ~~covers~~. In particular, the extreme deposition area is greater
 357 than the area of heavy deposition in the UP scenario. Further analysis shows that ~~the~~ extreme, moderate, and light deposition
 358 ~~area~~areas decrease in the order of UP, PP, and EP. The heavy deposition area shows the opposite trend, mainly attributed to the
 359 ~~checking~~check dams and ~~slope protection with~~ vegetation ~~revetments~~.



360



361

362 **Figure 6: (a) Simulated geomorphic changes over time for the three scenarios; (b) The affected area of deposition and erosion for**
 363 **the three scenarios; (c) The columnar distribution of different erosion and deposition levels.**

364 **4.3 Details of key locations**

365 As shown in Fig. 7, the controlling control measures and surroundings for the three scenarios are further investigated. Behind
 366 the two dams upriver in Scenarios PP and EP, the evident orange clusters indicate deposition. In contrast, these locations are
 367 dominated by erosion, shown in green, in scenario UP. Further analysis of the sediment depth shown in Fig. 8 shows that the
 368 deposited depth behind the dams in Scenario EP is lower than that in Scenario PP. Additionally, in Scenario PP, sediment
 369 trapped by dam 1 is less than that of dam 2, but both have deposition thicknesses of more than 10 m, which exceed the dams'
 370 heights (dam 1's height is 10 m, dam 2's height is 9 m). For the simulation results in Scenario EP, the values of deposition
 371 depth behind the two dams are nearly 8 m, which is lower than the dams' heights.

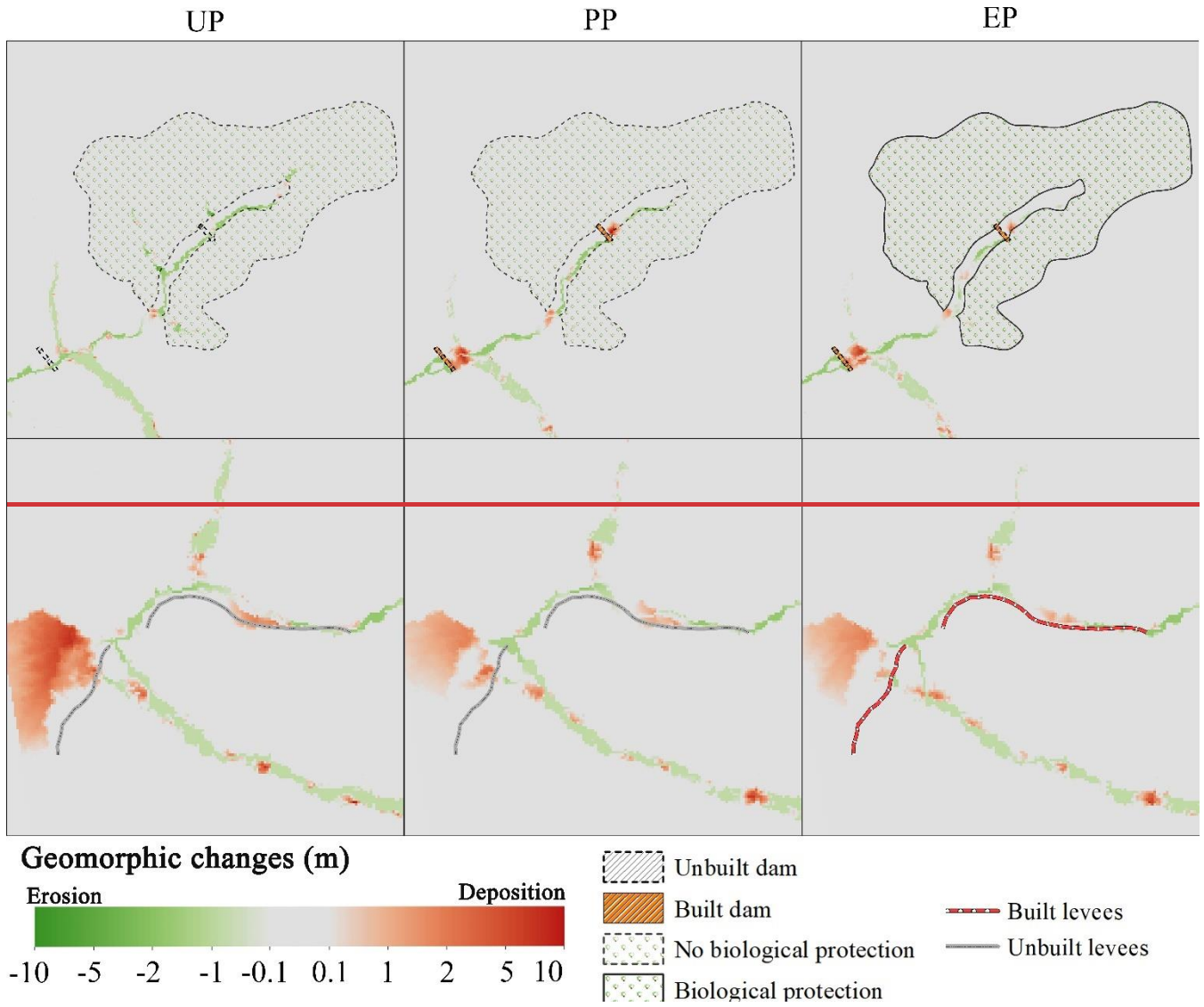
372 The additional biological ecological protection measure alters the material produced from the upriver tributary gullies. A sedi-
 373 ment volume of $14.4 \times 10^4 \text{ m}^3$ is transported from the biological protection area vegetated slopes in the EP scenario (solid lines
 374 in Fig. 7). A total of $27.1 \times 10^4 \text{ m}^3$ and $16.9 \times 10^4 \text{ m}^3$ of loose material are produced in the same region without biological ecolog-
 375 ical protection in Scenarios UP and PP, respectively. The vegetation revetment vegetated slopes enhances sediment conserva-
 376 tion based on the role of in conjunction with dam 1. Compared with the deposition in UP and PP without levees in the downriver

377

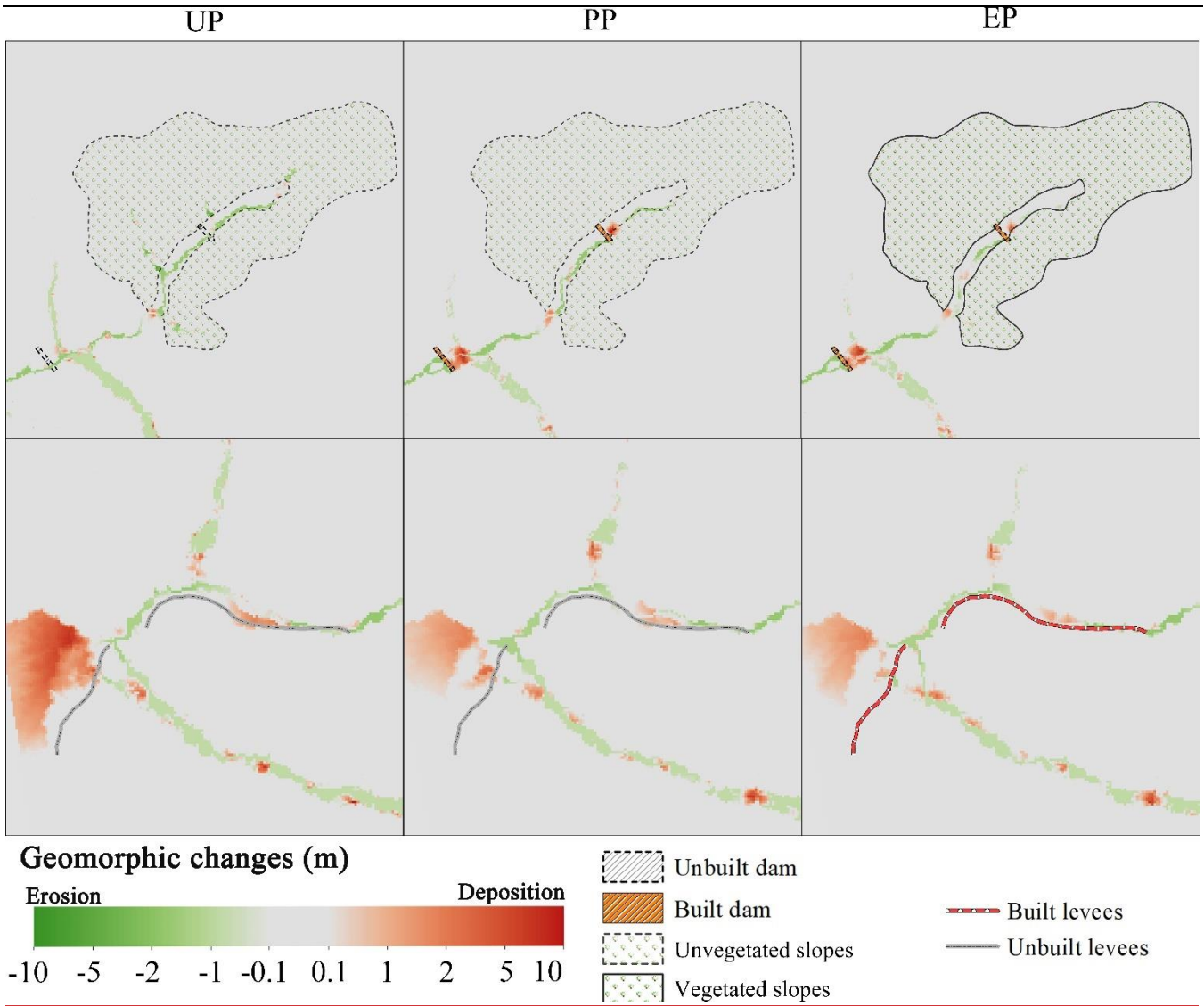
area (shown in the bottom row of Fig. 7), the levees in EP block debris in the bend of the channel and play an essential role in

378

protecting the residents and cultivated land behind the levees.



379



380

381

382

383

Figure 7: Geomorphic changes at key locations of the simulation results for the UP, PP, and EP scenarios. The top row is the upriver extent containing dam 1, dam 2 and the ~~vegetation revegetment~~ vegetated slopes. The bottom row is the downriver extent containing levees.

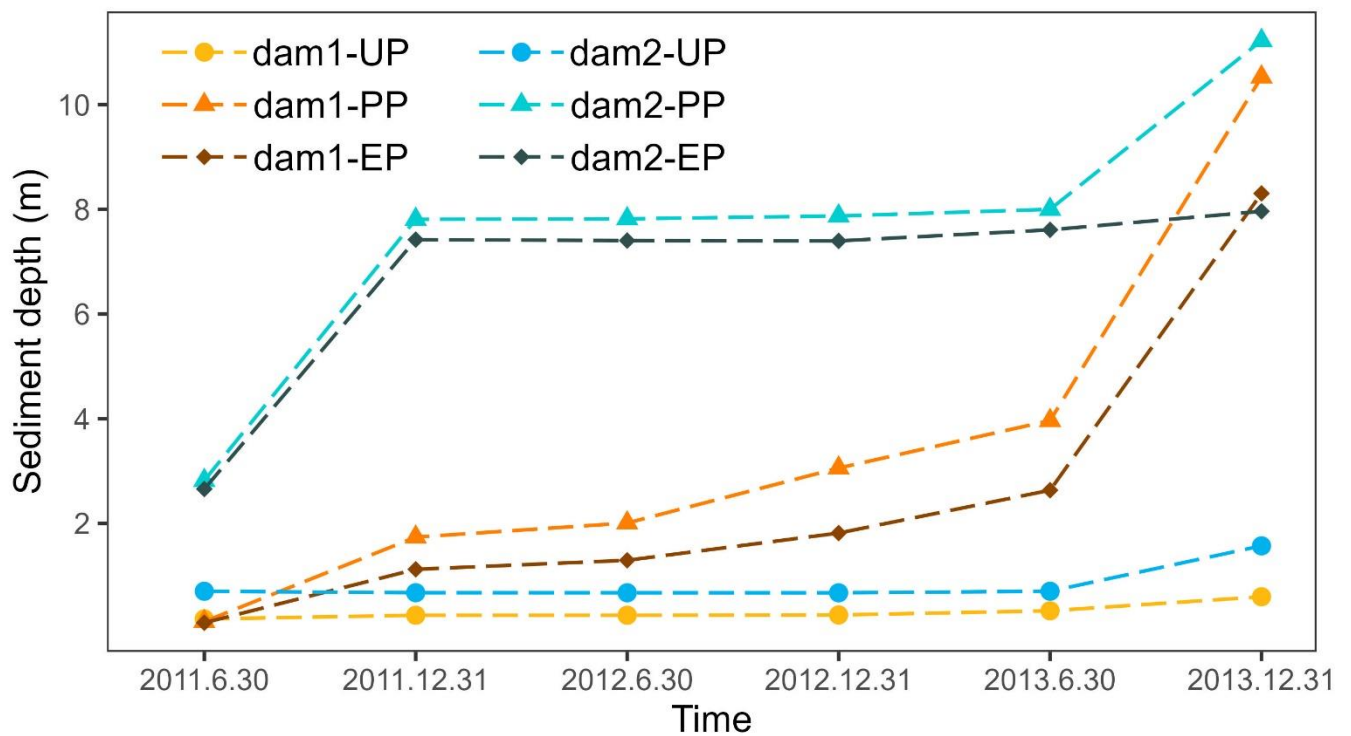
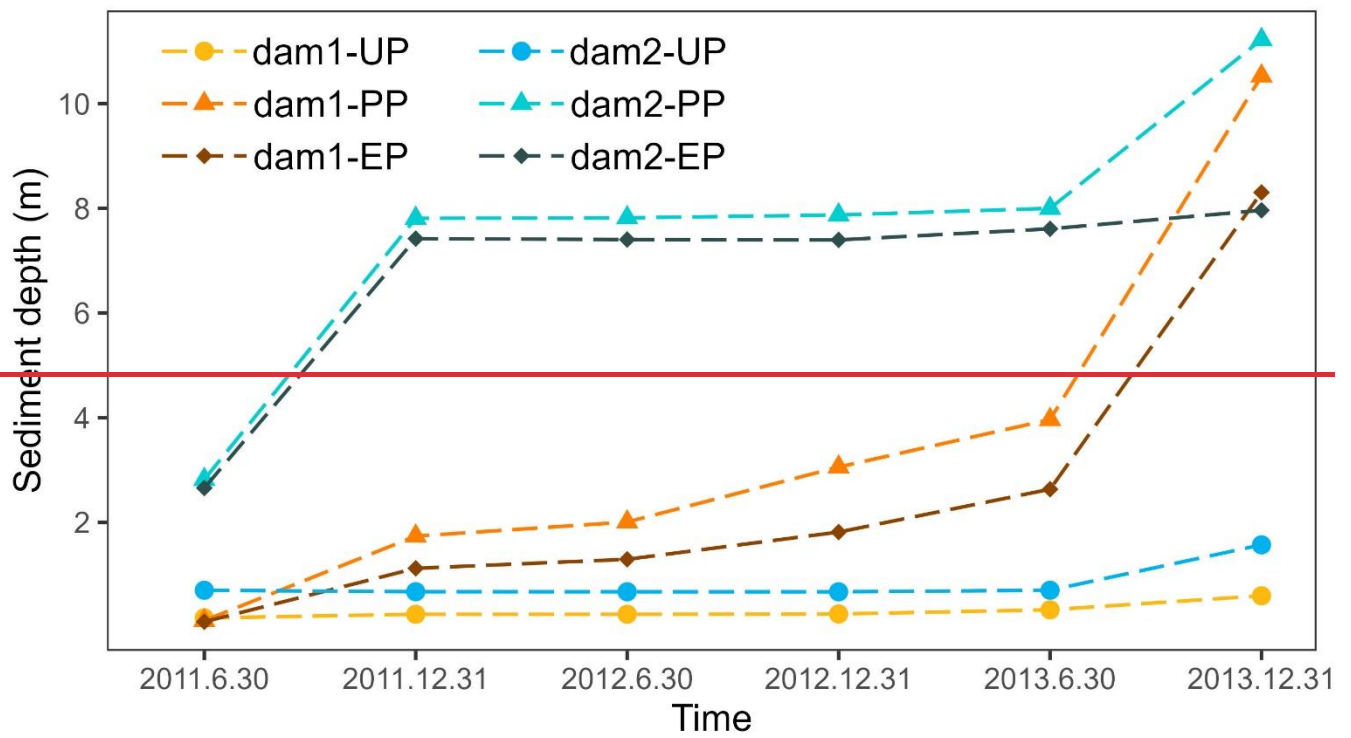


Figure 8: The depth of deposited sediment in the dams' placements.

4.4 Effectiveness assessment of the intervention measures

Figure 9 shows the erosion and deposition volumes in the source, transitional, and depositdeposition areas and compares the conservation ability (Ca) in each scenario. For all three scenarios, the deposition volume in the source area is less than that in the transitional area, and the largest amount of sediment is accumulated in the depositdeposition area. Regarding the eroded sediment, the largest volume is in the transitional area, followed by the transitional area, and the source area presents

the lowest volume. Moreover, sediment transport is best controlled in the depositdeposition area and worst contained in the source area under any intervention conditions.

Compared with the Ca of the source area in Scenario UP, the value increases by 138.1% in Scenario PP, which is attributed to dam+dam 1. Likewise, dam 2 in the transitional area effectively reduces sediment loss, which is reflected by a 52.5% increase in Ca . Furthermore, the mitigation measures in Scenario PP with vegetation revegetated slopes and levees in Scenario EP act best. The conservation ability in the source area increased by 161.9% due to the dam retainment and slope protection with vegetation-revetment, and the levees helped increase the Ca by 3.49% in the depositdeposition area.

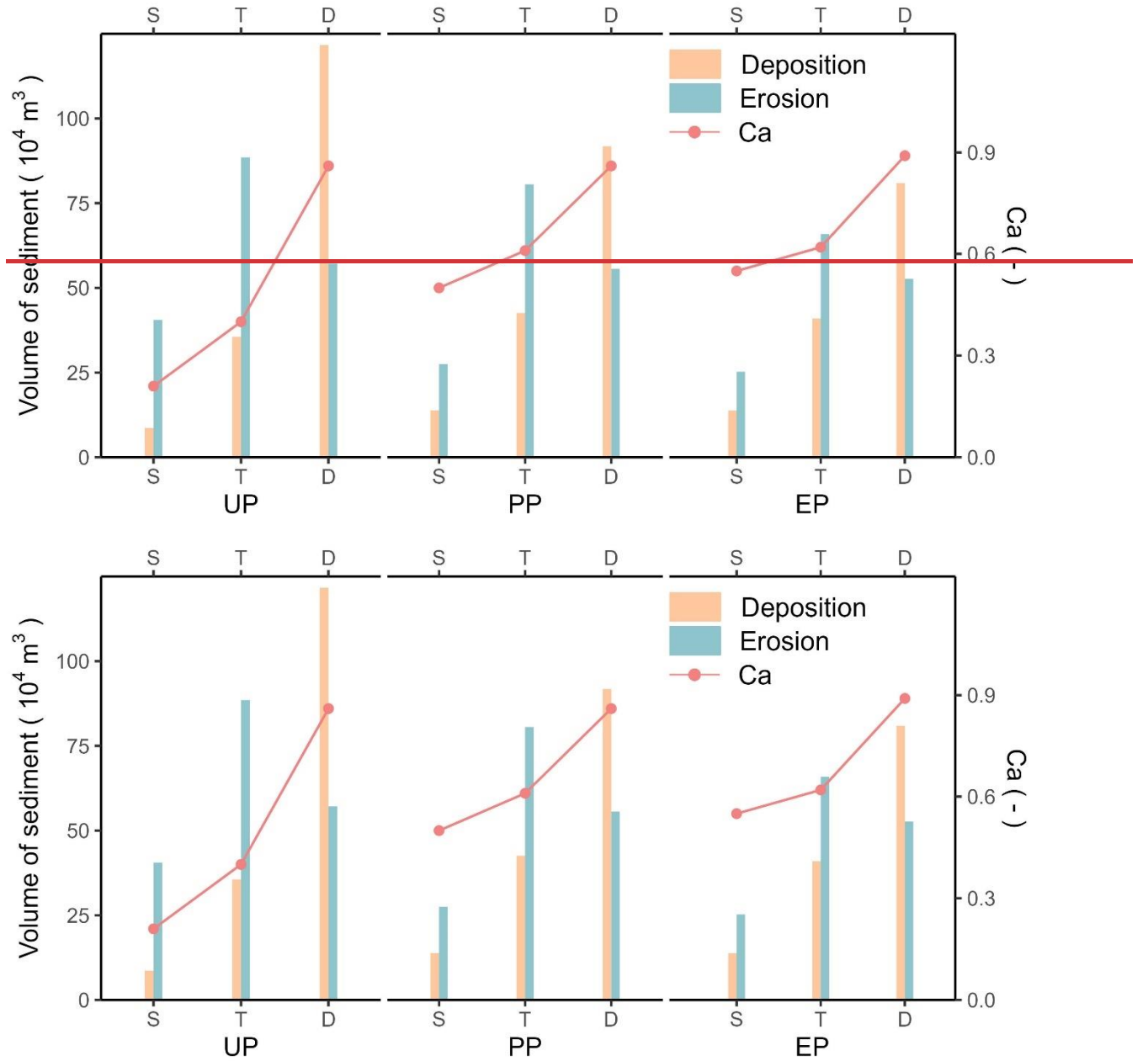
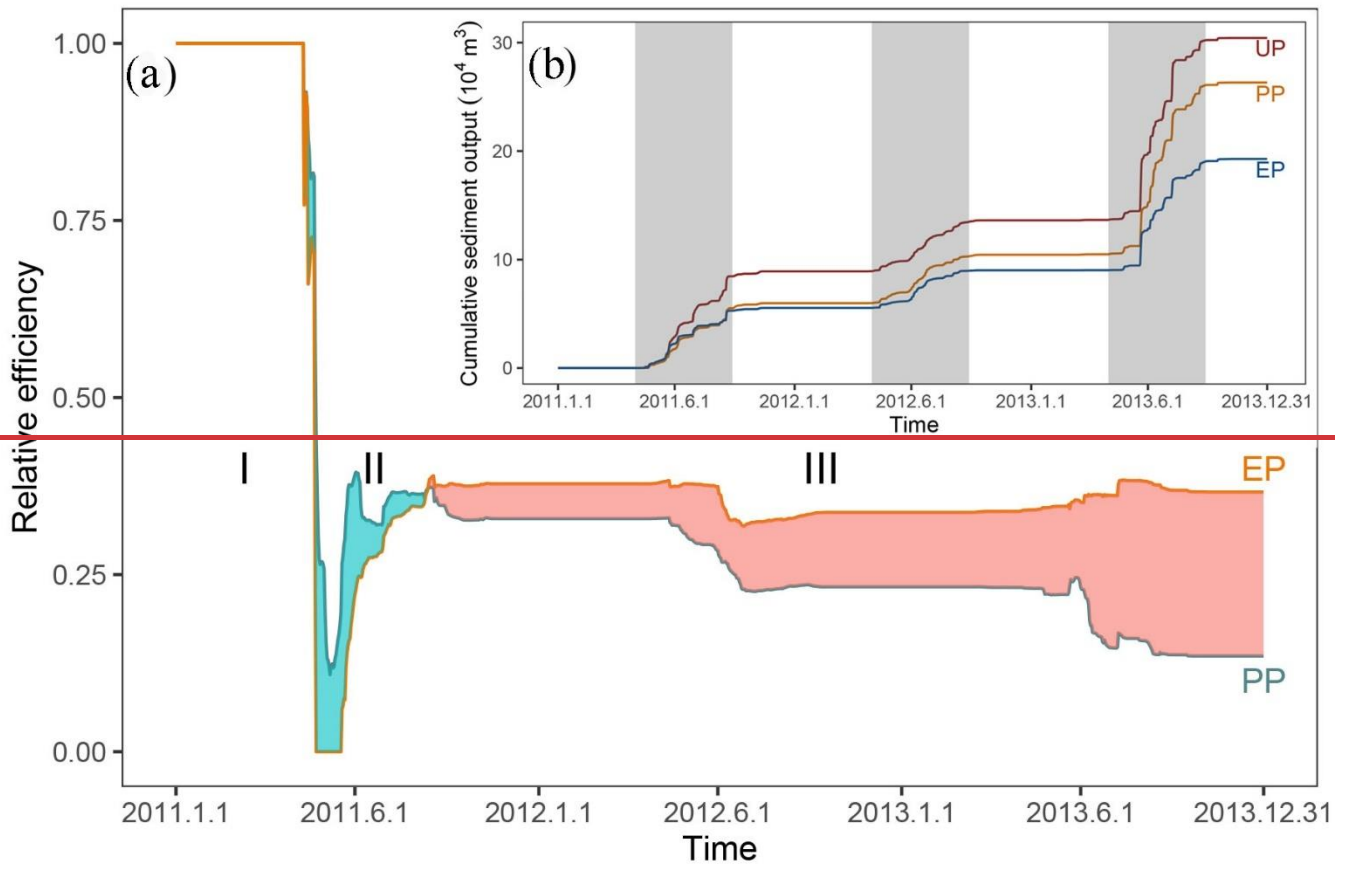


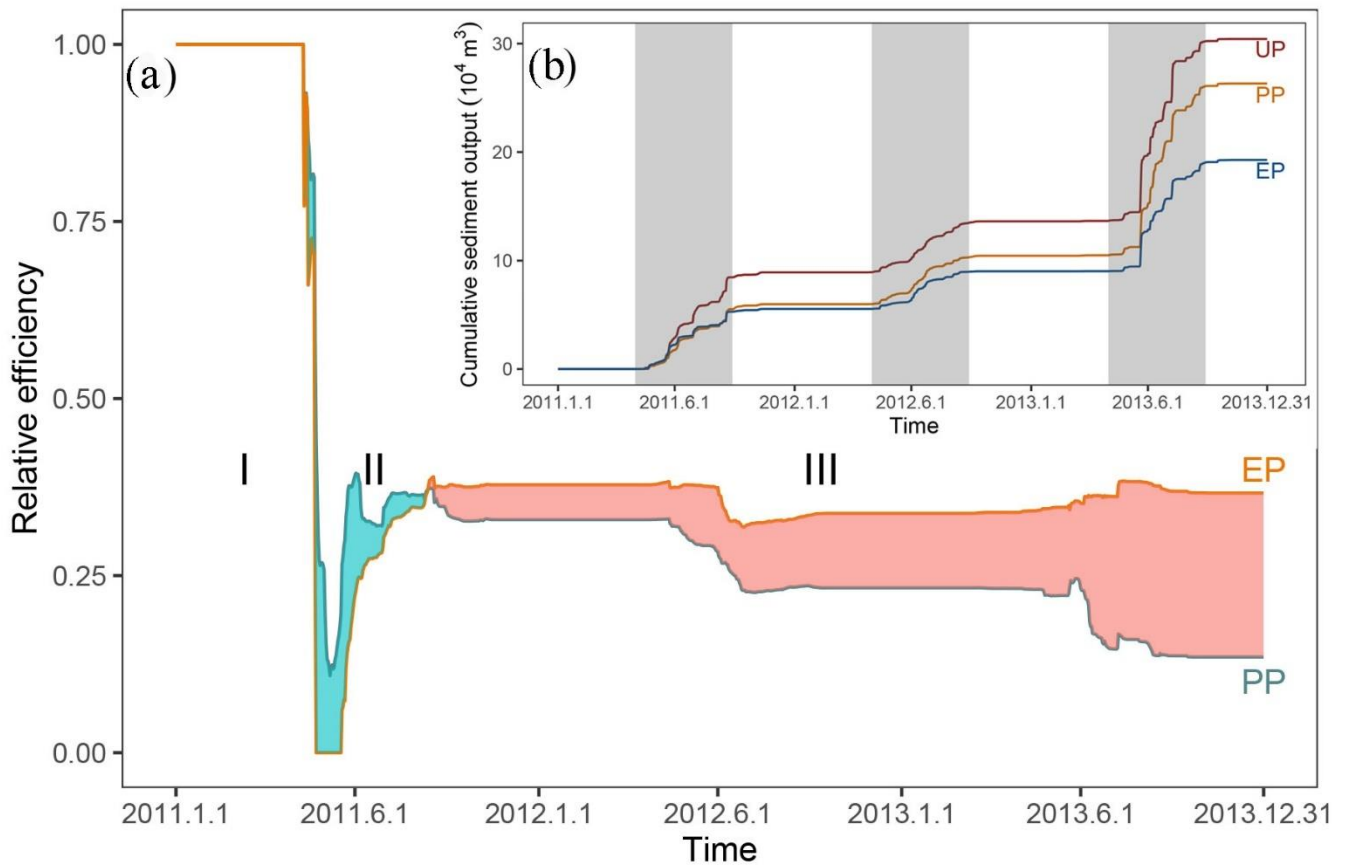
Figure 9: The volumes of sediment and the conservation ability (Ca) in the three areas for each scenario (S: source area; T: transitional area; D: depositdeposition area).

The cumulative sediment yield time series for each scenario and the relative efficiency of scenarios UP and EP are presented in Fig. 10b and Fig. 10a, respectively. The steep curve of the output cumulative sediment indicates a significant increase in the deposition. Three increasing stages are consistent with the rainfall intensity in the three monsoons (May-Sept). The total sediment output in UP is the largest at $\sim 30.4 \times 10^4 \text{ m}^3$, followed by the sediment yield of PP at $26.3 \times 10^4 \text{ m}^3$, and EP produced the least material at $19.3 \times 10^4 \text{ m}^3$.

408 The relative efficiency over the period of controlling measures by human intervention in PP and EP (Fig. 10a) indicates three
409 distinct stages. Stage I shows that the intervention measures in both scenarios completely prevent sediment transport. Later,
410 stage II shows a peculiar period when the effect of enhanced protective measures in EP ~~pales in comparison with~~ less than
411 that in PP through repeated experiments. ~~For~~In stage III, the relative efficiency of the intervention measures in EP is greater
412 than that in UP, which achieves the long-term effect and stable conservation of solid material.



413



414
 415 **Figure 10: (a) Relative efficiency efficiencies of Scenarios UP and EP compared with the that of Scenario UP (cyan shading represents**
 416 **when PP is more effective than EP and red shading represents the opposite); (b) Cumulative sediment yield over time (grey region**
 417 **highlighting three monsoons).**

418 **5. Discussion**

419 **5.1 Model calibration and uncertainty**

420 Calibration and uncertainty analysis are essential important issues in the CAESAR-Lisflood (C-L) simulation of the geo-
 421 morphic response to intervention measures based on the CA framework (Yeh and Li, 2006). A preliminary calibration was
 422 carried out in our study by reproducing the geomorphic changes and water depth driven by an extreme rainfall event that
 423 occurred in 2018. The results (Fig. S3) demonstrated that the C-L model successfully can well replicated the flash flood event
 424 using the initial conditions and model parameters. And the The calibration of the geomorphic response to the intervention
 425 measures was derived from a direct comparison between the model results and direct observed measurements (Fig. 4 and Fig.
 426 5). As a result, the simulated water discharge was more greater than the measured discharge but with on the same order of
 427 magnitude. Moreover, the errors of erosion and deposition depth between the simulation in Scenario PP and photographic
 428 evidence at three locations were less than 20%. The These results suggest the robustness of the model settings and parameter-
 429 isation.

430 The source of uncertainty is mainly from the model parameters and driving factors. Skinner et al. (2018b) provided a detailed
 431 sensitivity analysis of C-L, indicating that the sediment transport formula significantly influences a smaller catchment mod-
 432 elled by 10 m grid cells. The sediment transport law and the Wilcock and Crowe equations (Wilcock et al., 2003) have been
 433 proven suitable in the Xingping valley (Xie et al., 2018, 2022a, b; Li et al., 2020). Nevertheless, the empirical models of
 434 sediment transport overpredict bedload transport rates in steep streams (gradients greater than 3%) (D'Agostino and Lenzi,
 435 1999; Yager et al., 2012). Additionally, the driving factor proved suitable in the Xingping valley (Xie et al., 2018, 2022a, b; Li

et al., 2020). Nevertheless, the empirical models of sediment transport overpredict bedload transport rates in steep streams (gradients greater than 3%) (D'Agostino and Lenzi, 1999; Yager et al., 2012). Additionally, the input hourly rainfall data downscaled from the daily sequence, is an unrealistic situation. Various sediment transport equations and downscaled hourly rainfall data need to be tested in the C-L model to further decrease uncertainty.

5.2 The intervention effects

In this study, more facilities create more comprehensive intervention systems which aim to control sediment delivery. The C-L model simulated the geomorphic responses to intervention measures and suggested the considerable influence of intervention measures on spatial modifications and sediment yield. The intervention measures lead to fewer total affected areas (7.9%-19.7%) and lower sediment yields (16.7%-36.7%), which are suggested in the overall evidence (see Fig. 6 and Fig. 10). The model's prediction of the overall catchment-scale dynamics due to extreme events is in line with the viewpoints of other authors (Chen et al., 2023; Lan et al., 2020; Chen et al., 2015).

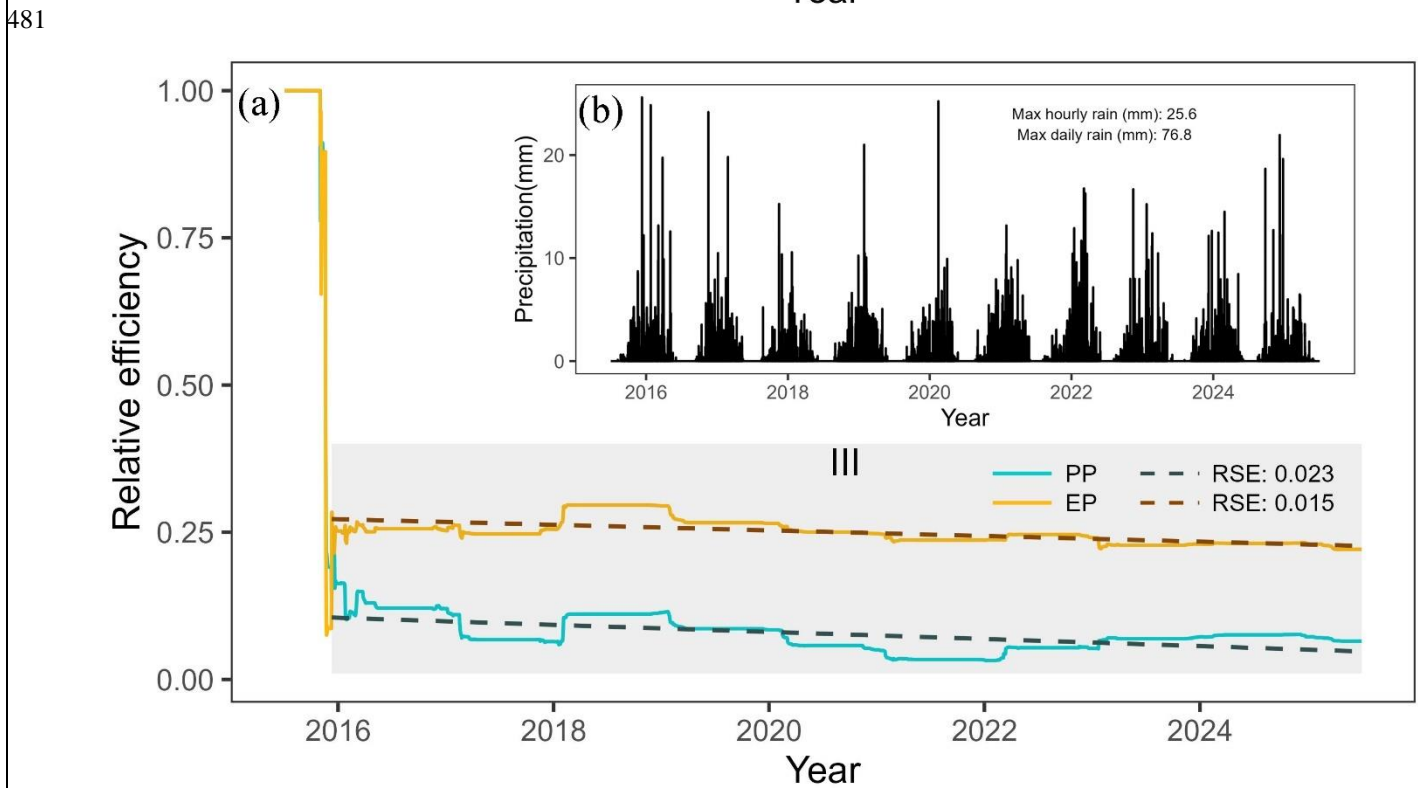
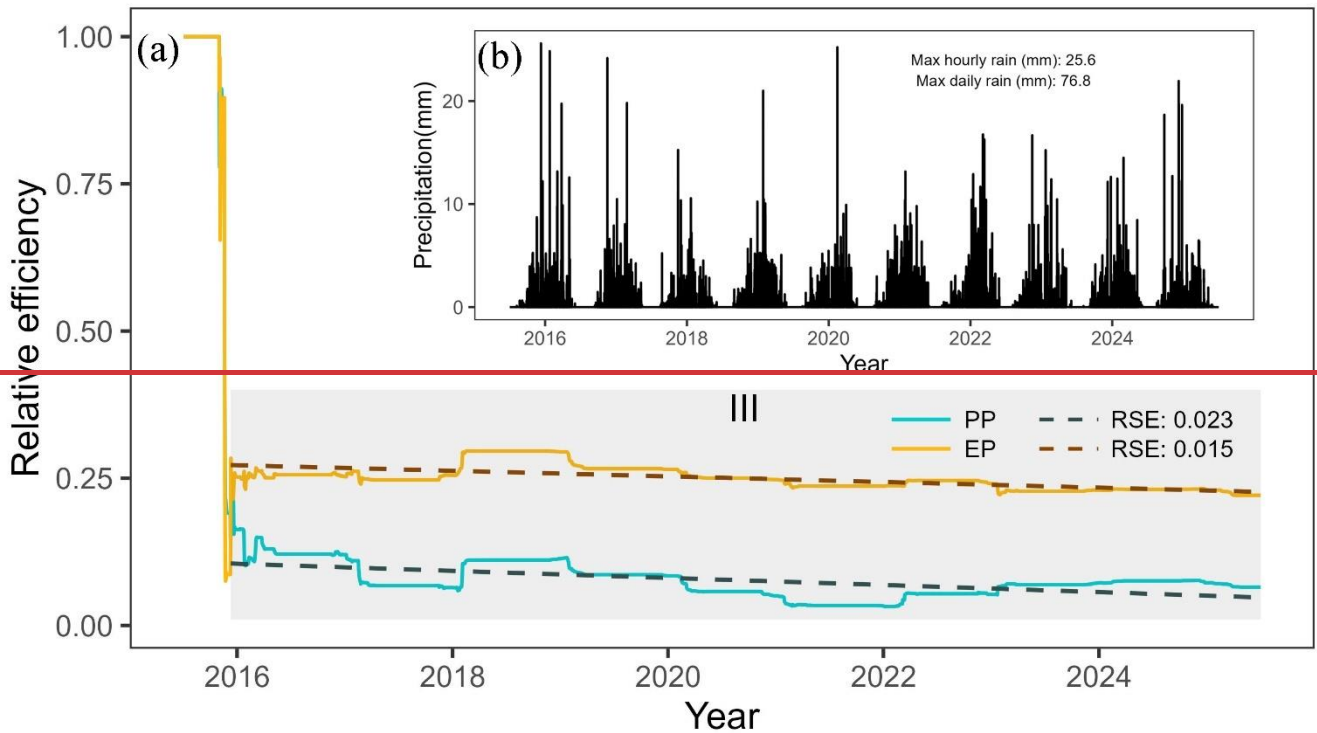
In this study, various measures were taken to represent three intervention scenarios with the goal of controlling sediment transport. The C-L model simulated the geomorphic responses to intervention measures and suggested the considerable influence of intervention measures on spatial modifications and sediment yield. The intervention measures lead to reductions in the total affected area (7.9%-19.7%) and lower sediment yields (16.7%-36.7%), as demonstrated by the overall evidence (see Fig. 6 and Fig. 10). The model's prediction of the overall catchment-scale dynamics in response to extreme events is in line with the viewpoints of other authors (Chen et al., 2023; Lan et al., 2020; Chen et al., 2015).

The mitigation measures considerably change the soil conservation ability considerably in the three-subregions including source area, transitional area and deposition zone, especially in the source area. We hypothesised that the two main reasons for the decreased erosion in the source area compared to the other two subregions, which can be inferred from caused by the interactions of loose material and topographic constraints. First, most of the abundant loose solid material formed triggered by the strong earthquake has stabilised overall since the 2008 debris flow (details in Table S1). Second, the long and deep gullies are mainly located in the transitional area (Yaogouli, Shicouzi, Yangjiashan) and deposit deposition area (Qinggangping), which). These gullies provide more a greater sediment supply than the source area. As shown in Fig. S4, the movement of the material occurs mainly in the branch valleys in the transitional and deposit deposition zones.

Moreover, morphological details changes and the ability of soil conservation ability of the in three scenarios show the unique role played by different intervention measures. For example, check dams are most effective in blocking sediment, and vegetation revegetated slopes can further strengthen the conservation ability. The synergetic effect of the soil conservation ability increases by more than two-fold due to the combination of the check dams and the vegetation coverage. increases the soil conservation ability by more than twofold. The levees are barriers with can pose a discernible impact on sediment conservation but with specific object-oriented protection.

The effectiveness of mitigation measures decreases over time with a smaller downward trend. We supplemented a. We performed an additional ten-year experiment to reveal the declining trend over an extended period. We randomly selected one of the 50 repeated rainfall datasets (year 2016-year 2025) downscaled by Li et al., 2020 Li et al., 2020, which were generated from the NEX-GDDP product (spatial resolution: $0.25^\circ \times 0.25^\circ$, temporal resolution: daily) under the RCP 4.5 emission scenario. The extracted rainfall sequence was then input into the C-L model to simulate the effectiveness of the three intervention scenarios. The result (Fig. 11) illustrates that stage III (the stable stage that started on the 161st day, in which Scenario EP's intervention measures were more effective) lasted longer than stages I and II. The relative effectiveness in both the PP and EP scenarios decreased gradually, while the curve fell faster in the PP scenario (slope: -1.65×10^{-5}) than in the EP scenario (slope: -1.31×10^{-5}).

476 The storage capacity of the ~~checkingcheck~~ dams ~~fade~~~~decreases~~ with ~~the~~ sediment ~~accumulated~~, ~~which~~ ~~accumulation~~, and ~~this~~
 477 ~~decrease~~ necessarily leads to a gradual ~~decrease~~~~reduction~~ in intervention effectiveness. ~~Additionally,However~~, ~~slope protection~~
 478 ~~with~~ vegetation ~~revetments remain~~~~remains~~ operationally effective in reducing sediment transport by stabilising topsoil over
 479 the period when the role of dam reservoirs gradually fails due to the lack of dredging work. Therefore, the vegetation protection
 480 strategy is vital for “green development” to reduce sediment loss but requires further efforts.



482
 483 **Figure 11: Rainfall input ~~of~~over ten years and relative efficiency of sediment intervention measures. (a) Relative efficiency changes**
 484 **over ten years (the grey region highlighting stage III, and the dashed lines indicate the linear fitting curves); (b) Rainfall downscaled**
 485 **from ~~the~~ NEX-GDDP (NASA Earth Exchange Global Daily Downscaled Projections) product.**

5.3 Limitations and applications

We built the dams and levees in our simulations by increasing the elevation in the expected location and assuming that it could not be eroded (see <https://sourceforge.net/projects/caesar-lisflood/>). This method proved experimentally feasible (Poepl et al., 2019; Gioia and Schiattarella, 2020). The rigid dam and levee body embedded in the model were not broken or weakened over time so that the simulation result could underestimate the geohazard risk. Considering the complexity of the geo-hazard mechanism, the abovementioned tools cannot simulate the occurrence process of geo-hazard chain links. They ignore the possible instantaneous damage to the environment and facilities downstream. Some typical geohazard chains have focused on specified events in the short term and recreated the hazard lifecycle using physical and mechanical models (Fan et al., 2020).

The methods applied in the study further demonstrate that the C-L model is an effective tool for understanding short to medium term or long term geomorphological changes (Ramirez et al., 2022; Li et al., 2020; Coulthard et al., 2012a) and observing the effectiveness of natural hazard intervention measures under different rainfall patterns. Our simulations indicate that the mitigation facilities in this study are effective, especially engineering efforts incorporating vegetation revetments in the upstream area, which would help decision makers optimise the management strategies to control mountain disasters. Geotechnical engineering has disadvantages, even though it is a mature technology that identifies and fixes problems quickly. We built the check dams and levees in our simulations by increasing the elevation in specific locations where they could not be eroded (see <https://sourceforge.net/projects/caesar-lisflood/>), which has been proved experimentally feasible (Poepl et al., 2019; Gioia and Schiattarella, 2020). The check dam and levee bodies embedded in the model were not broken or weakened over time so that the simulation result could underestimate the geo-hazard risks. Considering the complexity of the geo-hazard mechanism, the abovementioned tools cannot simulate the occurrence process of geo-hazard chain links. They ignore the possible instantaneous damage to the environment and facilities downstream.

The methods applied in the study further demonstrate that the C-L is an effective tool for understanding short-medium term or long-term geomorphic changes (Ramirez et al., 2022; Li et al., 2020; Coulthard et al., 2012a) and testing the effectiveness of intervention measures under different scenarios. Our simulations indicate that the mitigation measures in this study are effective, especially the combination of check dam and vegetated slopes in the upstream area, which could help decision-makers optimise the management strategies to control mountain disasters. Though geotechnical engineering is a mature technology that can effectively prevent geo-hazard occurrence (Cui and Lin, 2013), such as the need for extensive labour and expense and the difficulty of maintenance. While “green development”, the planting and maintenance of vegetation cover can effectively prevent erosion by strengthening topsoil and absorbing excess rainwater via roots (Reichenbach et al., 2014; Stokes et al., 2014; Forbes and Broadhead, 2013; Mickovski et al., 2007). Alternatively, these methods can be used to study tree planting patterns on different slopes.

It has disadvantages such as extensive cost and the difficulty of maintenance. In “green development”, the planting and maintenance of vegetation cover can effectively prevent erosion by strengthening topsoil and absorbing excess rainwater via roots (Reichenbach et al., 2014; Stokes et al., 2014; Forbes and Broadhead, 2013; Mickovski et al., 2007). Alternatively, these methods can be used to study the impact of tree planting patterns on sediment dynamics.

6. Conclusions

In this study, scenarios involving check dams, biological measures vegetated slopes and artificial barriers were simulated using the C-L model to outline the erosion and deposition areas, measure the impacts of sediment blocking sediment, and retention, thus examine how vegetation revetments vegetated slope help stabilise slopes. Four key findings are concluded, were ob-

524 ~~tained~~. First, the geotechnical engineering ~~measures~~ used for controlling sediment transport are efficient, and ~~the~~their perfor-
525 mance in protecting the fragile environment can be improved by ~~combining these engineering efforts~~integrating with other
526 intervention measures, such as ~~vegetation revetments~~ecological engineering and artificial barriers. Second, the effectiveness
527 of mitigation measures decreases over time. Third, the characteristics of the sediment transport patterns ~~alter~~are considerably
528 altered due to the intervention measures. The stabilising sediment ability in the source area increased by 161.9% with the
529 additional effect of slope protection with ~~vegetation revetments~~. ~~Finally, To sum up,~~ the present intervention measures need to
530 be ~~revised to reduce erosion and should be combined with~~ refined with regular dredging ~~work~~works to maintain the effective-
531 ness of reducing sediment transport.

532 Declaration of interest statement

533 The authors declare that they have no known competing financial interests or personal relationships that could have appeared
534 to influence the work reported in this paper.

535 Author contribution

536 Di Wang: Conceptualisation, Methodology, Software, Writing-original draft preparation. Ming Wang Kai Liu and Jun Xie:
537 Supervision, Methodology, Writing- Reviewing and Editing, Validation.

538 Acknowledgements

539 This research was supported by the National Key Research and Development Plan (2017YFC1502902). The financial support
540 is highly appreciated. The authors would also like to thank Professor Tom Coulthard and his team for their excellent work on
541 the freely available C-L model (<https://sourceforge.net/projects/caesar-lisflood>).

542 Reference

543 References

- 544 Bates, P. D., Horritt, M. S., and Fewtrell, T. J.: A simple inertial formulation of the shallow water equations for efficient
545 two-dimensional flood inundation modelling, *J. Hydrol.*, 387, 33–45, <https://doi.org/10.1016/j.jhydrol.2010.03.027>, 2010.
- 546 ~~Batty, M. and Xie, Y.: Possible urban automata, *Environ. Plan. B Plan. Des.*, 24, 175–192, <https://doi.org/10.1068/b240175>,~~
547 ~~1997.~~
- 548 Beven, K.: Linking parameters across scales: subgrid parameterizations and scale dependent hydrological models, *Hydrol.*
549 *Process.*, 9, 507–525, <https://doi.org/https://doi.org/10.1002/hyp.3360090504>, 1995.
- 550 Beven, K.: TOPMODEL:A critical, *Hydrol. Process.*, 11, 1069–1085, [https://doi.org/https://doi.org/10.1002/\(SICI\)1099-](https://doi.org/https://doi.org/10.1002/(SICI)1099-)
551 [1085\(199707\)11:9<1069::AID-HYP545>3.0.CO;2-O](https://doi.org/https://doi.org/10.1002/(SICI)1099-1085(199707)11:9<1069::AID-HYP545>3.0.CO;2-O), 1997.
- 552 Beven, K. J. and Kirkby, M. J.: A physically based, variable contributing area model of basin hydrology, *Hydrol. Sci. Bull.*,
553 24, 43–69, <https://doi.org/10.1080/02626667909491834>, 1979.
- 554 Chen, N., Zhou, H., Yang, L., Yang, L., and Lv, L.: Analysis of benefits of debris flow control projects in southwest
555 mountains areas of China, *J. Chengdu Univ. Technol. (Science Technol. Ed.)*, 40, 50–58, <https://doi.org/10.3969/j.issn.1671->
556 [9727.2013.01.008](https://doi.org/10.3969/j.issn.1671-9727.2013.01.008), 2013.

557 Chen, X., Li, Z., Cui, P., and Liu, X.: Estimation of soil erosion caused by the 5.12 Wenchuan Earthquake, *J. Mt. Sci.*, 27,
558 122–127, 2009.

559 Chen, X., Cui, P., You, Y., Chen, J., and Li, D.: Engineering measures for debris flow hazard mitigation in the Wenchuan
560 earthquake area, *Eng. Geol.*, 194, 73–85, <https://doi.org/10.1016/j.enggeo.2014.10.002>, 2015.

561 Chen, Y., Li, J., Jiao, J., Wang, N., Bai, L., Chen, T., Zhao, C., Zhang, Z., Xu, Q., and Han, J.: Modeling the impacts of
562 fully-filled check dams on flood processes using CAESAR-lisflood model in the Shejiagou catchment of the Loess Plateau,
563 China, *J. Hydrol. Reg. Stud.*, 45, 101290, <https://doi.org/10.1016/j.ejrh.2022.101290>, 2023.

564 Cong, K., Li, R., and Bi, Y.: Benefit evaluation of debris flow control engineering based on the FLO-2D model, *Northwest
565 Geol.*, 52, <https://doi.org/10.19751/j.cnki.61-1149/p.2019.03.019>, 2019.

566 ~~Couclelis, H.: From cellular automata to urban models: new principles for model development and implementation, *Environ-
567 Plan. B Plan. Des.*, 24, 165–174, <https://doi.org/10.1068/b240165>, 1997.~~

568 Coulthard, T. J. and Skinner, C. J.: The sensitivity of landscape evolution models to spatial and temporal rainfall resolution,
569 *Earth Surf. Dyn.*, 4, 757–771, <https://doi.org/10.5194/esurf-4-757-2016>, 2016.

570 Coulthard, T. J. and Wiel, Van De J., M.: Modelling long term basin scale sediment connectivity, driven by spatial land use
571 changes, *Geomorphology*, 277, 265–281, <https://doi.org/10.1016/j.geomorph.2016.05.027>, 2017.

572 Coulthard, T. J., Macklin, M. G., and Kirkby, M. J.: A cellular model of Holocene upland river basin and alluvial fan
573 evolution, *Earth Surf. Process. Landforms*, 27, 269–288, <https://doi.org/10.1002/esp.318>, 2002.

574 Coulthard, T. J., Hancock, G. R., and Lowry, J. B. C.: Modelling soil erosion with a downscaled landscape evolution model,
575 *Earth Surf. Process. Landforms*, 37, 1046–1055, <https://doi.org/10.1002/esp.3226>, 2012a.

576 Coulthard, T. J., Ramirez, J., Fowler, H. J., and Glenis, V.: Using the UKCP09 probabilistic scenarios to model the amplified
577 impact of climate change on drainage basin sediment yield, *Hydrol. Earth Syst. Sci.*, 16, 4401–4416,
578 <https://doi.org/10.5194/hess-16-4401-2012>, 2012b.

579 Coulthard, T. J., Neal, J. C., Bates, P. D., Ramirez, J., de Almeida, G. A. M., and Hancock, G. R.: Integrating the
580 LISFLOOD-FP 2D hydrodynamic model with the CAESAR model: Implications for modelling landscape evolution, *Earth
581 Surf. Process. Landforms*, 38, 1897–1906, <https://doi.org/10.1002/esp.3478>, ~~2013~~2013a.

582 ~~Coulthard, T. J., Neal, J. C., Bates, P. D., Ramirez, J., de Almeida, G. A. M., and Hancock, G. R.: Integrating the
583 LISFLOOD-FP 2D hydrodynamic model with the CAESAR model: Implications for modelling landscape evolution, *Earth
584 Surf. Process. Landforms*, 38, 1897–1906, <https://doi.org/10.1002/esp.3478>, 2013b.~~

585 Cui, P. and Lin, Y.: Debris-Flow Treatment: The Integration of Botanical and Geotechnical Methods, *J. Resour. Ecol.*, 4,
586 097–104, <https://doi.org/10.5814/j.issn.1674-764x.2013.02.001>, 2013.

587 Cui, P., Zhou, G. G. D., Zhu, X. H., and Zhang, J. Q.: Scale amplification of natural debris flows caused by cascading
588 landslide dam failures, *Geomorphology*, 182, 173–189, <https://doi.org/10.1016/j.geomorph.2012.11.009>, 2013.

589 D’Agostino, V. and Lenzi, M. A.: Bedload transport in the instrumented catchment of the Rio Cordon. Part II: Analysis of
590 the bedload rate, *Catena*, 36, 191–204, [https://doi.org/10.1016/S0341-8162\(99\)00017-X](https://doi.org/10.1016/S0341-8162(99)00017-X), 1999.

591 Einstein, H. A.: The Bed-Load Function for Sediment Transportation in Open Channel Flows, 1950.

592 Fan, X., Yang, F., Siva Subramanian, S., Xu, Q., Feng, Z., Mavrouli, O., Peng, M., Ouyang, C., Jansen, J. D., and Huang, R.:
593 Prediction of a multi-hazard chain by an integrated numerical simulation approach: the Baige landslide, Jinsha River, China,
594 *Landslides*, 17, 147–164, <https://doi.org/10.1007/s10346-019-01313-5>, 2020.

595 Feng, W., He, S., Liu, Z., Yi, X., and Bai, H.: Features of Debris Flows and Their Engineering Control Effects at Xinping
596 Gully of Pingwu County, *J. Eng. Geol.*, 25, <https://doi.org/10.13544/j.cnki.jeg.2017.03.027>, 2017.

597 Forbes, K. and Broadhead, J.: Forests and landslides: the role of trees and forests in the prevention of landslides and
598 rehabilitation of landslide-affected areas in Asia, FAO, 14–18 pp., 2013.

599 Gioia, D. and Schiattarella, M.: Modeling Short-Term Landscape Modification and Sedimentary Budget Induced by Dam
600 Removal: Insights from LEM Application, *Appl. Sci.*, 10, 7697, <https://doi.org/10.3390/app10217697>, 2020.

601 Goldberg, D. E.: Genetic Algorithms in Search, Optimization, and Machine Learning, Addison-Wesley Longman Publishing
602 Co., Inc., 372 pp., <https://doi.org/10.1007/BF01920603>, 1989.

603 Gorum, T., Fan, X., van Westen, C. J., Huang, R. Q., Xu, Q., Tang, C., and Wang, G.: Distribution pattern of earthquake-
604 induced landslides triggered by the 12 May 2008 Wenchuan earthquake, *Geomorphology*, 133, 152–167,
605 <https://doi.org/10.1016/j.geomorph.2010.12.030>, 2011.

606 Guo, Q., Xiao, J., and Guan, X.: The characteristics of debris flow activities and its optimal timing for the control in Shikan
607 River Basin Pingwu Country, *Chinese J. Geol. Hazard Control*, 29, <https://doi.org/10.16031/j.cnki.issn.1003-8035>. 2018.
608 03. 05, 2018.

609 Hancock, G. R., Verdon-Kidd, D., and Lowry, J. B. C.: Soil erosion predictions from a landscape evolution model – An
610 assessment of a post-mining landform using spatial climate change analogues, *Sci. Total Environ.*, 601–602, 109–121,
611 <https://doi.org/10.1016/j.scitotenv.2017.04.038>, 2017.

612 He, J., Zhang, L., Fan, R., Zhou, S., Luo, H., and Peng, D.: Evaluating effectiveness of mitigation measures for large debris
613 flows in Wenchuan, China, *Landslides*, 19, 913–928, <https://doi.org/10.1007/s10346-021-01809-z>, 2022.

614 Huang, R.: Geohazard assessment of the Wenchuan earthquake, Science Press, Beijing, 944 pp., 2009.

615 Huang, R. and Fan, X.: The landslide story, *Nat. Geosci.*, 6, 325–326, <https://doi.org/10.1038/ngeo1806>, 2013.

616 J.B.C. Lowry, M. Narayan, G.R. Hancock, and K.G. Evans: Understanding post-mining landforms: Utilising pre-mine
617 geomorphology to improve rehabilitation outcomes, *Geomorphology*, 328, 93–107,
618 <https://doi.org/10.1016/j.geomorph.2018.11.027>, 2019.

619 Lan, H., Wang, D., He, S., Fang, Y., Chen, W., Zhao, P., and Qi, Y.: Experimental study on the effects of tree planting on
620 slope stability, *Landslides*, 17, 1021–1035, <https://doi.org/10.1007/s10346-020-01348-z>, 2020.

621 Lee, T. and Jeong, C.: Nonparametric statistical temporal downscaling of daily precipitation to hourly precipitation and
622 implications for climate change scenarios, *J. Hydrol.*, 510, 182–196, <https://doi.org/10.1016/j.jhydrol.2013.12.027>, 2014.

623 Li, C., Wang, M., and Liu, K.: A decadal evolution of landslides and debris flows after the Wenchuan earthquake,
624 *Geomorphology*, 323, 1–12, <https://doi.org/10.1016/j.geomorph.2018.09.010>, 2018.

625 Li, C., Wang, M., Liu, K., and Coulthard, T. J.: Landscape evolution of the Wenchuan earthquake-stricken area in response
626 to future climate change, *J. Hydrol.*, 590, 125244, <https://doi.org/10.1016/j.jhydrol.2020.125244>, 2020.

627 Marchi, L., Comiti, F., Crema, S., and Cavalli, M.: Channel control works and sediment connectivity in the European Alps,
628 *Sci. Total Environ.*, 668, 389–399, <https://doi.org/10.1016/j.scitotenv.2019.02.416>, 2019.

629 Mickovski, S. B., Bengough, A. G., Bransby, M. F., Davies, M. C. R., Hallett, P. D., and Sonnenberg, R.: Material stiffness,
630 branching pattern and soil matric potential affect the pullout resistance of model root systems, *Eur. J. Soil Sci.*, 58, 1471–
631 1481, <https://doi.org/10.1111/j.1365-2389.2007.00953.x>, 2007.

632 Poepl, R. E., Coulthard, T., Keesstra, S. D., and Keiler, M.: Modeling the impact of dam removal on channel evolution and
633 sediment delivery in a multiple dam setting, *Int. J. Sediment Res.*, 34, 537–549, <https://doi.org/10.1016/j.ijsrc.2019.06.001>,
634 2019.

635 Ramirez, J. A., Zischg, A. P., Schürmann, S., Zimmermann, M., Weingartner, R., Coulthard, T., and Keiler, M.: Modeling
636 the geomorphic response to early river engineering works using CAESAR-Lisflood, *Anthropocene*, 32,
637 <https://doi.org/10.1016/j.ancene.2020.100266>, 2020.

638 Ramirez, J. A., Mertin, M., Peleg, N., Horton, P., Skinner, C., Zimmermann, M., and Keiler, M.: Modelling the long-term
639 geomorphic response to check dam failures in an alpine channel with CAESAR-Lisflood, *Int. J. Sediment Res.*, 37, 687–700,
640 <https://doi.org/10.1016/j.ijsrc.2022.04.005>, 2022.

641 Reichenbach, P., Busca, C., Mondini, A. C., and Rossi, M.: The Influence of Land Use Change on Landslide Susceptibility
642 Zonation: The Briga Catchment Test Site (Messina, Italy), *Environ. Manage.*, 54, 1372–1384,
643 <https://doi.org/10.1007/s00267-014-0357-0>, 2014.

644 Saynor, M. J., Lowry, J. B. C., and Boyden, J. M.: Assessment of rip lines using CAESAR-Lisflood on a trial landform at the
645 Ranger Uranium Mine, *L. Degrad. Dev.*, 30, 504–514, <https://doi.org/10.1002/ldr.3242>, 2019.

646 Skinner, C. J., Coulthard, T. J., Schwanghart, W., Van De Wiel, M. J., and Hancock, G.: Global sensitivity analysis of
647 parameter uncertainty in landscape evolution models, *Geosci. Model Dev.*, 11, 4873–4888, [https://doi.org/10.5194/gmd-11-](https://doi.org/10.5194/gmd-11-4873-2018)
648 4873-2018, 2018a.

649 Skinner, C. J., Coulthard, T. J., Schwanghart, W., Van De Wiel, M. J., and Hancock, G.: Global sensitivity analysis of
650 parameter uncertainty in landscape evolution models, *Geosci. Model Dev.*, 11, 4873–4888, [https://doi.org/10.5194/gmd-11-](https://doi.org/10.5194/gmd-11-4873-2018)
651 4873-2018, 2018b.

652 Slingerland, N., Beier, N., and Wilson, G.: Stress testing geomorphic and traditional tailings dam designs for closure using a
653 landscape evolution model, in: *Proceedings of the 13th International Conference on Mine Closure*, 1533–1544,
654 https://doi.org/10.36487/ACG_rep/1915_120_Slingerland, 2019.

655 Stokes, A., Douglas, G. B., Fourcaud, T., Giadrossich, F., Gillies, C., Hubble, T., Kim, J. H., Loades, K. W., Mao, Z.,
656 McIvor, I. R., Mickovski, S. B., Mitchell, S., Osman, N., Phillips, C., Poesen, J., Polster, D., Preti, F., Raymond, P., Rey, F.,
657 Schwarz, M., and Walker, L. R.: Ecological mitigation of hillslope instability: Ten key issues facing researchers and
658 practitioners, *Plant Soil*, 377, 1–23, <https://doi.org/10.1007/s11104-014-2044-6>, 2014.

659 Thomson, H. and Chandler, L.: Tailings storage facility landform evolution modelling, in: *Proceedings of the 13th*
660 *International Conference on Mine Closure*, 385–396, https://doi.org/10.36487/ACG_rep/1915_31_Thomson, 2019.

661 Wang, M., Yang, W., Shi, P., Xu, C., and Liu, L.: Diagnosis of vegetation recovery in mountainous regions after the
662 wenchuan earthquake, *IEEE J. Sel. Top. Appl. Earth Obs. Remote Sens.*, 7, 3029–3037,
663 <https://doi.org/10.1109/JSTARS.2014.2327794>, ~~2014a~~2014.

664 ~~Wang, M., Liu, M., Yang, S., and Shi, P.: Incorporating Triggering and Environmental Factors in the Analysis of~~
665 ~~Earthquake Induced Landslide Hazards, *Int. J. Disaster Risk Sci.*, 5, 125–135, <https://doi.org/10.1007/s13753-014-0020-7>,~~
666 ~~2014b.~~

667 Wang, N., Han, B., Pang, Q., and Yu, Z.: post-evaluation model on effectiveness of debris flow control, *J. Eng. Geol.*, 23,
668 219–226, <https://doi.org/10.13544/j.cnki.jeg.2015.02.005>, 2015.

669 Van De Wiel, M. J., Coulthard, T. J., Macklin, M. G., and Lewin, J.: Embedding reach-scale fluvial dynamics within the
670 CAESAR cellular automaton landscape evolution model, *Geomorphology*, 90, 283–301,
671 <https://doi.org/10.1016/j.geomorph.2006.10.024>, 2007.

672 Wilcock, P. R., Asce, M., and Crowe, J. C.: Surface-based Transport Model for Mixed-Size Sediment Surface-based
673 Transport Model for Mixed-Size Sediment, 9429, [https://doi.org/10.1061/\(ASCE\)0733-9429\(2003\)129](https://doi.org/10.1061/(ASCE)0733-9429(2003)129), 2003.

674 Xie, J., Wang, M., Liu, K., and Coulthard, T. J.: Modeling sediment movement and channel response to rainfall variability
675 after a major earthquake, *Geomorphology*, 320, 18–32, <https://doi.org/10.1016/j.geomorph.2018.07.022>, 2018.

676 Xie, J., Coulthard, T. J., and McLelland, S. J.: Modelling the impact of seismic triggered landslide location on basin
677 sediment yield, dynamics and connectivity, *Geomorphology*, 398, 108029, <https://doi.org/10.1016/j.geomorph.2021.108029>,
678 2022a.

679 Xie, J., Coulthard, T. J., Wang, M., and Wu, J.: Tracing seismic landslide-derived sediment dynamics in response to climate
680 change, *Catena*, 217, 106495, <https://doi.org/10.1016/j.catena.2022.106495>, 2022b.

681 Xu, C., Xu, X., Yao, X., and Dai, F.: Three (nearly) complete inventories of landslides triggered by the May 12, 2008
682 Wenchuan Mw 7.9 earthquake of China and their spatial distribution statistical analysis, *Landslides*, 11, 441–461,
683 <https://doi.org/10.1007/s10346-013-0404-6>, 2014.

684 Yager, E. M., Turowski, J. M., Rickenman, D., and McArdeell, B. W.: Sediment supply, grain protrusion, and bedload
685 transport in mountain streams, *Geophys. Res. Lett.*, 39, 1–5, <https://doi.org/10.1029/2012GL051654>, 2012.

686 Yang, Z., Duan, X., Huang, J., Dong, Y., Zhang, X., Liu, J., and Yang, C.: Tracking long-term cascade check dam siltation:
687 implications for debris flow control and landslide stability, *Landslides*, 18, 3923–3935, [https://doi.org/10.1007/s10346-021-](https://doi.org/10.1007/s10346-021-01755-w)
688 [01755-w](https://doi.org/10.1007/s10346-021-01755-w), 2021.

689 Yeh, A. G. O. and Li, X.: Errors and uncertainties in urban cellular automata, *Comput. Environ. Urban Syst.*, 30, 10–28,
690 <https://doi.org/10.1016/j.compenurbsys.2004.05.007>, 2006.

691 Yu, B., Yang, Y., Su, Y., Huang, W., and Wang, G.: Research on the giant debris flow hazards in Zhouqu County, Gansu
692 Province on August 7, 2010, *J. Eng. Geol.*, 18, 437–444, <https://doi.org/10.3969/j.issn.1004-9665.2010.04.001>, 2010.

693 Zhang, L. and Liang, K.: Research on economic benefit evaluation of the prevention and cure project for debris flow,
694 *Chinese J. Geol. Hazard Control*, 16, 48–53, <https://doi.org/10.3969/j.issn.1003-8035.2005.03.011>, 2005.

695 ~~Zhang, X., Wang, M., Liu, K., Xie, J., and Xu, H.: Using NDVI time series to diagnose vegetation recovery after major~~
696 ~~earthquake based on dynamic time warping and lower bound distance, *Ecol. Indic.*, 94, 52–61,~~
697 ~~<https://doi.org/10.1016/j.ecolind.2018.06.026>, 2018.~~

698 Zhou, H., Chen, N., Lu, Y., and Li, B.: Control Effectiveness of Check Dams in Debris Flow Gully: A Case of Huashiban
699 Gully in Earthquake Worst-stricken Area, Beichuan County, *J. Mt. Sci.*, 30, 347–354, [https://doi.org/10.3969/j.issn.1008-](https://doi.org/10.3969/j.issn.1008-2786.2012.03.015)
700 [2786.2012.03.015](https://doi.org/10.3969/j.issn.1008-2786.2012.03.015), 2012.

701